ASSESSMENT OF LEVELS OF NATURAL RADIOACTIVITY IN SURFACE SOILS AROUND TITANIUM MINES IN KENYA

BY

MASORE, KEFA OSORO
REG. NO.: I56/7246/2002

DEPARTMENT OF PHYSICS

A thesis submitted in partial fulfilment of the requirements for the award of the degree of Master of Science in the School of Pure and Applied Sciences of Kenyatta University.

15 September 2007

DECLARATION

This thesis is my original work and has not been presented for the award of a degree or any other award in any University.

All sources of information have particularly been acknowledged by way of references.

..... Sign

24/1/07 ..... Date

Masore, Kefa Osoro
(I56/7246/2002)
Department of Physics,
Kenyatta University
P.O. Box 43844,
Nairobi, KENYA.

We confirm that the candidate, under our supervision, carried out the work reported in this thesis.

Prof. I. V. S. Rathore,
Department of Physics,
Kenyatta University,
P.O. Box 43844,
Nairobi, KENYA.

..... Sign

24/09/07 ..... Date

Dr. Amidu O. Mustapha,
Department of Physics,
University of Nairobi,
P.O. Box 30197,
Nairobi, KENYA.

..... Sign

24/09/07 ..... Date

Mr. Michael J. Mangala,
Institute of Nuclear Science,
University of Nairobi
P.O. Box 30197,
Nairobi, KENYA.

..... Sign

24/9/2007 ..... Date

DEDICATION

To my mother, my wife and our dear children

ACKNOWLEDGEMENTS

I take great pleasure in acknowledging the support received from the following who jointly and severally made invaluable contributions towards the success of this thesis.

First, I greatly thank the university supervisors: Prof. I. V. S. Rathore (Department of Physics, Kenyatta University), Dr. Amidu O. Mustapha (Department of Physics, University of Nairobi) and Mr. Michael J. Mangala (Institute of Nuclear Science and Technology, University of Nairobi) for their guidance and direction. The ideas and knowledge presented in this thesis were shaped by countless discussions with these radiation experts, without whose supervision very little would have been achieved regarding the research project. They read thesis drafts in time and always availed themselves to share their experiences, insights and opinions despite their obviously tight schedules. Special thanks also to Mr. Willis Ambuso of Department of Physics, Kenyatta University for advice that always came handy.

Gratefully, I acknowledge the assistance of the chairman/director and staff and students of the Department of Physics, Kenyatta University and the Institute of Nuclear Science and Technology, University of Nairobi for permission to use their respective experimental equipment. The chairman of Department of Physics of Kenyatta University always ensured that any necessary external help was obtained in good time.

Am also grateful for the assistance I received from the following institutions: the Institute of Nuclear Science and Technology, University of Nairobi for availing their laboratory equipment for analysis of samples; Ministry of Education, Nairobi for

authorising the research in a short time; the Office of the President through the Kwale District Commissioner and the Msambweni District Officer for permission to collect soil samples from the study area and the United Nations Environmental Programme (UNEP), Nairobi for access and use of library and internet facilities for literature on the study subject.

Further gratitude go to Mr. William Angwenyi, Mr. Chris Kanoti, Mr. Richard Maroko, Mr. Stanley Areba and the bodaboda (taxi) operators of Msambweni for their kind assistance during sample collection. Many thanks go to Madam Ann Maina of the Department of Physics and to Madam Flora and Mr Musakala both of Materials Research and Laboratory, Ministry of Roads and Public Works, for assistance in the preparation of soil samples for testing and analysis.

Last but not least, I am highly grateful to my mother, my wife and my children for their unlimited material and moral support, love and encouragement.

TABLE OF CONTENTS

Content	Page
Title	(i)
Declaration	(ii)
Dedication	(iii)
Acknowledgements	(iv)
Table of Contents	(vi)
Abstract	(ix)
List of Figures	(x)
List of Tables	(xi)
List of Abbreviations	(xii)
List of Symbols and Units	(xiii)
Chapter 1: Introduction	**1**
1.1 Backgrounds to the Study	1
1.1.1 The Titanium Mines in Kenya	1
1.1.2 Geology and Geomorphology of the Area of Study	3
1.2 Statement of the Research Problem	5
1.3 Objectives of the Research Project	6
1.4 Significance of the Research Project	7
Chapter 2: Literature Review	**8**
2.1 Environmental Radioactivity	8
2.2 Human Exposures to Environmental Radioactivity	11
2.3 Biological Effects of Radioactivity	12
2.4 Environmental Radioactivity Studies in Kenya	15
Chapter 3: Theoretical Background of Gamma-ray Spectrometry	**17**

3.1 Emission of Gamma Rays by Radioactive Nuclei 17
3.2 Interaction of Gamma Radiation with Matter 17
3.2.1 Photoelectric Effect 18
3.2.2 Compton Effect 19
3.2.3 Pair Production 20
3.3 Principles of Gamma-ray Spectrometry 21
3.4 Radiation Dose From Terrestrial Exposure 23
Chapter 4: Materials and Methods **25**
4.1 Sampling and Preparation of Samples 25
4.2 The Experimental Procedure 27
4.2.1 Experimental Gamma-Ray Spectrometry System 27
4.2.2 Energy Calibration of the Spectrometer System 28
4.2.3 Sample Counting 29
4.2.4 Calculation of Radioactivity 30
4.2.5 Detection Limits 30
4.3 Gamma Radiation Dose Rates 31
Chapter 5: Results and Discussion **32**
5.1 Quality Control and Assurance 32
5.2 Radioactivity Concentrations of Radionuclides 34
5.3 Human Exposure to Gamma Radiation 44
Chapter 6: Conclusions and Recommendations **50**
6.1 Conclusion 50
6.2 Recommendations 51
References **52**
Appendices **56**

Appendix 1: Gamma-Ray Spectrum of Standard Reference Material (SRM-1) 56

Appendix 2: ^{238}U Decay Series 57

Appendix 3: ^{232}Th Decay Series 58

Appendix 4: Typical Gamma Spectrum of Soil Sample 59

ABSTRACT

All human beings are exposed to radiation from naturally occurring radionuclides in soil and other environmental materials. Some of these exposures are not amenable to control and they are usually referred to as background radiation. Some work activities such as conventional mining inadvertently produce large quantities of naturally occurring radionuclides, which can result in additional and/or elevated levels of radiation exposure of people in the areas around the mining sites. Such exposures - induced or enhanced by human activities - are subject to control by regulatory authorities. In some instances there may be contributions from the two types of exposures and they must be separated before applying regulatory control. In this study, natural radioactivity levels in surface soils around the proposed titanium mines in Kwale district were determined from measurements of 78 samples of surface soils randomly sampled from two villages within the proposed mining area by using a hyper pure germanium (HpGe) gamma-ray spectrometer. The values of radioactivity concentrations in the soils and the likely radiation doses from contact with these soils were determined and are reported in this thesis. The radiological implication of these levels is discussed with regards to the impending mining operations in the area. The ranges and mean of radioactivity concentrations ($Bqkg^{-1}$) obtained are: 8.4±0.4-43.6±1.5 (27.6±1.7) for ^{232}Th; 7.4±0.6-40.6±1.4 (20.9±1.5) for ^{226}Ra and 31.9±1.3-114.1±1.4 (69.5±3.2) for ^{40}K, respectively. The likely absorbed dose rates in air above these soils were calculated from these radioactivity concentrations and found to be 8.5±0.5-36.9±1.1 $nGyh^{-1}$ with a mean of 25.2±1.4 $nGyh^{-1}$. The corresponding effective dose rates are 21.0±1.2-90.8±2.6 μSvy^{-1} with a mean of 62.0±3.5 μSvy^{-1}, which are lower than the global average of 0.46 $mSvy^{-1}$ and therefore of little radiological risk to the environment of the study subject.

LIST OF FIGURES

Fig. 3.1:	Photoelectric emission of an electron	18
Fig. 3.2:	Compton Scattering of a gamma photon	19
Fig. 3.3:	The Process of Pair Production	20
Fig. 4.1a:	Sampling Map and Profile	26
Fig. 4.1b:	Sampling and Sample Analysis Scheme	27
Fig. 4.2:	Schematic diagram of HpGe detection system	28
Fig. 5.1:	Correlation of measured values with certified values of radioactivity of reference materials	34
Fig. 5.2:	Typical gamma-ray spectrum of a soil sample	35
Fig. 5.3a:	^{232}Th radioactivity levels in soil	40
Fig. 5.3b:	^{226}Ra radioactivity levels in soil	41
Fig. 5.3c:	^{40}K radioactivity levels in analyzed soil	41
Fig. 5.4a:	Variation of radioactivity concentration of ^{232}Th with that of ^{226}Ra	43
Fig. 5.4b:	Variation of radioactivity concentration of ^{232}Th with that of ^{40}K	43
Fig. 5.4c:	Correlation of radioactivity concentration of ^{226}Ra with that of ^{40}K	44
Fig. 5.5:	Contributions of ^{226}Ra, ^{232}Th and ^{40}K to gamma radiation dose rate	47
Fig. 5.6a:	Distribution of absorbed dose rate ($nGyh^{-1}$) in the analyzed soil samples	48
Fig. 5.6b:	Distribution of effective dose rate (μSvy^{-1}) in analyzed soil samples	48

LIST OF TABLES

Table 2.1:	Primordial radionuclides with their half-lives and relative abundance/activity	9
Table 2.2:	Cosmogenic radionuclides with their half-lives and activity	10
Table 2.3:	Man-made radionuclides and their half-lives and sources	11
Table 2.4:	Annual radiation dose limits recommended by the ICRP	15
Table 5.1:	Mean detection limits of the HpGe Detector.	32
Table 5.2:	Measured and certified values of radioactivity of the reference materials RGTh-1, RGU-1, and RGK-1.	33
Table 5.3a:	Radioactivity concentration of ^{232}Th in soil samples	36
Table 5.3b	Radioactivity concentration of ^{226}Ra (^{238}U) in soil samples	37
Table 5.3c:	Radioactivity concentration of ^{40}K in soil samples	38
Table 5.4:	Minimum, maximum and mean radioactivity concentrations of ^{232}Th, ^{226}Ra and ^{40}K in Soil	39
Table 5.5:	Absorbed and effective gamma radiation dose rates in soil.	45
Table 5.6:	Minimum, maximum and mean absorbed and effective gamma radiation dose rates in the tested soil samples	46

LIST OF ABBREVIATIONS

Term	Meaning
ARPANSA	Australian Radiation Protection and Nuclear Safety Agency
CES	Costal and Environmental Services
FEP	Full Energy Peak
FWHM	Full Width at Half Maximum; Resolution of the HpGe detector
GANAAS	Gamma spectrum analysis, Activity calculations and Neutron Activation Analysis Software
HpGe	Hyper pure germanium detector
IAEA	International Atomic Energy Agency
ICRP	International Commission on Radiological Protection
JICA	Japanese International Cooperation Agency
KTM	Kwale Titanium Mines
MCA	Multi-Channel Analyzer
NORM	Naturally Occurring Radioactive Materials
RGK-1	Standard Reference Material for Radioactivity of Potassium-40
RGTh-1	Standard Reference Material for Radioactivity of Thorium-232
RGU-1	Standard Reference Material for Radioactivity of Uranium-238
SRM	Standard Reference Material
UNEP	United Nations Environment Programme
UNSCEAR	United Nations Scientific Committee on Effects of Atomic Radiation

LIST OF SYMBOLS AND UNITS

Symbol	Meaning
^{129}I	Iodine-129
^{131}I	Iodine-131
^{137}Cs	Caesium-137
^{14}C	Carbon-14
^{208}Tl	Thallium-208
^{212}Pb	Lead-212
^{214}Bi	Bismuth-214
^{214}Pb	Lead-214
^{222}Rn	Radon-222
^{226}Ra/Ra-226	Radium-226
^{228}Ac	Actinium-228
^{232}Th/Th-232	Thorium-232
^{235}U/U-235	Uranium-235
^{238}U/U-238	Uranium-238
^{239}Pu	Plutonium-239
^{241}Am	Americium-241
^{3}H	Tritium
^{40}K/K-40	Potassium-40
^{60}Co	Cobalt-60
^{7}Be	Beryllium-7
^{90}Sr	Strontium-90
TiO_2	Titanium Oxide
μSvy^{-1}	Microsievert per year
$Bqkg^{-1}$	Becquerel per kilogram
Gy	Gray (Unit of Absorbed Dose Deposited on Unit Mass of Material; 1 Gy = 1 Jkg^{-1})
Gyh^{-1}	Gray per hour; Unit of absorbed dose
keV	Kiloelectronvolt (Unit of Energy = $1.6x10^{-19}$ J)
MeV	Megaelectronvolt (= 10^6 Electron Volts or $1.6x10^{-13}$ J)
Sv	Sievert (Unit of Effective Radiation Dose)
$mSvy^{-1}$	Millisievert per year

Chapter 1

Introduction

1.1 BACKGROUND TO THE STUDY

1.1.1 The Titanium Mines in Kenya

Rapid growth of the world population over the last several decades, currently exceeding the six billion mark (UNEP, 1999), and technological advancements, have increased the needs to exploit natural resources like metallic minerals, petroleum, wood and natural gas among others. Human activities such as mining and milling of materials containing naturally occurring radionuclides (NORM) may alter the natural distribution of these radionuclides in the environment.

A heavy mineral (titanium) mining operation is proposed for Kidiani and Mwaweche areas, east of Shimba Hills Settlement in Msambweni Division of Kwale District, Kenya. The proposed mining area is located approximately 65 km south of Mombasa Island and 10 km from the Indian Ocean. It stretches from approximately $39^0$26" E to approximately $39^0$30" E latitude and from approximately $4^0$23" S to approximately $4^0$30" S longitude, covering an area of about 20 km^2 (Figure 4.1a). The mineral ore is in two areas, which are separated by the Mukurumudzi River and the Ramisi Sugar Estate. The two mineral deposit areas include the two villages of Nguluku and Maumba, which will be affected by the mining project. It is estimated that the mineral deposits at Maumba, also known as the Kwale Central Dune, cover an area of 2 km^2 while those at Nguluku (also called the Kwale South Dune) cover an area of 3 km^2 (CES, 2000). About 3,000 people live in the area covered by the proposed titanium-mining project (Ong'olo, 2001). In both areas, the minerals occur as large sand dunes

that are locally concentrated and abundant in some places. The depth of the mineral deposits varies from 30 metres below the surface to 40 metres below the surface.

The mining area is in the tropics and, therefore, experiences reasonably constant temperatures throughout the year. The warmer temperatures are between November and April when they range from 26^0C to 28^0C (CES, 2000), while the cooler temperatures are between May and October when they range from 24^0C to 26^0C. The area experiences bimodal rainfall with long rains occurring from March to July and short rains from October to December. The area receives an average of 1300 mm of rainfall per year. During the rainy season the wind blows westwards bringing moisty air from the Indian Ocean and consequently rains, while during the dry season the northeast monsoon is dominant.

According to the project's mining proposal by the mining company, Tiomin Kenya, each of the mineral deposits will be mined in about seven years, beginning with the (Central dune) Maumba deposits. The ore body is estimated to contain 3-6% heavy minerals and 15-30% fine particles. The rest of the ore body is red or orange coloured sand. The total estimated resource is 1 million tonnes of rutile, 0.6 million tonnes of zircon and 4 million tonnes of ilmenite (CES, 2000). Rutile, zircon and ilmenite minerals appear in both Maumba and Nguluku as heavy sands (CES, 2000). These minerals are normally deposited at similar sites through sedimentation in riverine and marine waters. Ilmenite (with 49-51% titanium oxide, TiO_2) is the dominant mineral present followed by rutile (with 95-96% titanium oxide, TiO_2). These two minerals are used to make either titanium metal or titanium oxide (a white non-toxic pigment) in a highly specialized, toxic and energy-consuming refining process that begins with a rutile concentrate.

Titanium is used to provide the white colour in paints and as filler in plastics, paper, toothpaste, and many medicinal tablets and in sunscreens. It is also used in making aeroplane bodies, artificial limbs and bones and heart pacemakers. Current global production of titanium is in the range 120,000 to 140,000 tonnes per annum. The proposed output of titanium from the Kwale project is about twice the world's titanium metal needs annually (Ong'olo, 2001). Zircon is used in the manufacture of ceramic tiles and in refractory and foundry industries. Thus rutile, zircon and ilmenite are the targets for titanium mining in the area under study.

Tiomin Kenya has also indicated that the main stages of the mining operation will include: construction and operation of the heavy mineral sands mine; construction and operation of a ship loading facility; extraction and processing of the minerals; and transportation by road of the final products from the mines to the ship loading facility at Shimoni, 35 km from the mining site.

The mining process will involve clearing the vegetation of the mining area, stockpiling the topsoil for future use in rehabilitation of the mined areas, dry mining by an excavator (e.g., Bucket Wheel Excavator, BWE) or scrapper, transporting the sand by conveyor belt to the wet plant for further processing and mixing the ore-bearing sand with water to form slurry from which the heavy metals will be separated. These mining processes have the potential for environmental pollution, mainly due to dispersal of dust and other materials from the actual mining sites to the surroundings.

1.1.2 Geology and Geomorphology of the Area of Study

The proposed titanium mining area in Kwale district lies approximately $4^0$23" S to approximately $4^0$30" S latitude, and approximately $39^0$26" E to approximately $39^0$30"

E longitude, extending over a length of about 10 km with an average width of about 2 km. It slopes gently and rises from sea level to an altitude of about 150 metres above sea level at the top of the hills. The Mukurumudzi River is the major surface water source in the area. This is a perennial river that flows from the northwest to the southeast and drains into the Indian Ocean near Gazi Bay. A large part of the mineral deposits area drains into the Mukurumudzi River while the eastern side of the Central Dune drains into the smaller Kidogoweni and Mtawa rivers.

According to Austromineral report (1978) on Kenya's coastal mineralization, Nguluku area is mainly comprised of Maji-ya-Chumvi formation and Igneous rocks both of Duruma group of formations. The other members of the Duruma group are Mariakani formation, Mazeras formation and Magarini formation, which forms a belt of low hills running parallel to the coast. The Magarini formation consists of red or orange sand dunes that were deposited during the Pliocene, 2 to 5 million years ago. The Mazeras sandstones, derived from the disintegration of the Mozambican Belt metamorphic rocks, provided the supply of heavy minerals to the Magarini sands.

The mineral deposits at Kwale comprise two large sand dunes: the Kwale Central Dune at Maumba and the Kwale South Dune at Nguluku (Figure 4.1a). The geological arrangement is such that the mineral ore body is considered to be of a vent by igneous activities of alkaline rock composed of the so-called "agglomerate". Niobium and rare earth metals are the main composites of the alkaline igneous rock. The same mineralization is reported in the Mrima-Jombo area under the same alkaline igneous conditions (Austromineral, 1978). Post-reef sediments and coral reef sediments in the area have been associated with zircon and limestone respectively. The vent is surrounded by a sequence of Maji-ya-Chumvi profile covered on top by

sandstone and Taurus sediments that consist of alluvium, colluvium, dune sands, and coral reef in that order from the top. The sandstone consists of dune sands and other sands also in that order.

Maji-ya-Chumvi Formation is divided into three members: Upper, Middle and Lower members. Shale and siltstone beds dominate lower and Middle members while the Upper member consists of sandstone beds. A high value content of salt has been reported in shale beds of Lower members. (The term "Maji-ya-Chumvi" means "salty water" in the local language.) Sandstone beds in Upper member are comprised of silty sandstone beds with flaggy texture and well-developed joints (JICA, 1993).

Before the commencement of a mining operation, which has the potential of impacting negatively on the natural environmental, there is always the need to obtain some baseline data, which will serve as reference for future environmental assessments. Therefore, in this study, the natural radioactivity levels in samples of surface soil around the proposed mining area were measured prior to commencement of the mining operations. This is important because once mining operations begin the opportunity to obtain such baseline data will be lost, making it difficult to do an accurate assessment of the radiological and the environmental impact of the mining operation.

1.2 STATEMENT OF THE RESEARCH PROBLEM

Conventional mining operations inadvertently produce large quantities of naturally occurring radionuclides because the ores of interest, for example copper, bauxite, titanium, phosphates, etc., are normally mineralised with primordial radionuclides, particularly potassium-40 (^{40}K), uranium-238 (^{238}U), and thorium-232 (^{232}Th). These

radionuclides, although not originally designed to produce environmental radiation hazard, result in the enhancement of natural radiation background around the mining area. The enhancement is mainly due to contamination of liquid effluents from the mines, leachants from tailings, atmospheric release of dust particles and radon exhalation, which could lead to elevated exposures of both workers and the general public. The principal exposure pathways are internal exposure from alpha particles following inhalation of airborne dust particles and inadvertent ingestion of radionuclides with food, water, etc., and external exposure to gamma radiation from the bulk residue and by-products.

It is necessary to establish the background levels of the radioactivity and radiation in the environment of the mining facility prior to commencement of the mining operations. The present study focussed at determining the pre-operational radioactivity concentrations of the natural radionuclides present in surface soils around the proposed titanium mines.

1.3 OBJECTIVES OF THE RESEARCH PROJECT

The following were the specific objectives of this study:

(i) To determine radioactivity concentrations of the naturally occurring radionuclides present in surface soils around the proposed titanium mines in Kwale district.

(ii) To calculate the radiation dose rates arising from the ambient levels of natural radioactivity in the surface soils around the proposed titanium mines.

1.4 SIGNIFICANCE OF THE RESEARCH PROJECT

It is normally expected that, during the mining operations, precautionary measures will be taken to avoid unnecessary occupational and/or public radiation exposures by adopting standard working procedures and installing appropriate engineering devices. However, it is also the obligation of the management of the mining operation and/or the national regulatory authority to ensure regular monitoring (personal and environmental) procedures required to assess the effectiveness of the existing exposure-control measures and to review the radiological impact of the mining operations. It is therefore necessary to establish the 'normal' background levels of the radioactivity in the area surrounding the proposed mining facilities prior to the commencement of the mining operations.

Chapter 2

Literature Review

2.1 ENVIRONMENTAL RADIOACTIVITY

Environmental radioactivity arises as a result of the presence of three categories of radionuclides: Primordial radionuclides (which have been in existence since the time of formation of the earth), cosmogenic radionuclides (which are formed as a result of cosmic ray interactions) and human-produced radionuclides (which are enhanced or formed due to human activities) (Radiation Information Network, 2004). These radionuclides are found naturally in air, water and soil. They are even found in the human body, which is made up of chemicals, some of them being radionuclides ingested daily with water and food.

Primordial radionuclides are leftovers from the time of formation of the earth. They are typically long-lived, with half-lives in the order of hundreds of millions of years. The progeny or decay products of these long-lived radionuclides are also in this category. Table 2.1 shows some basic information on some of the common primordial radionuclides (Radiation Information Network, 2004).

Generally the primordial radionuclides are evenly distributed in rocks and soils everywhere around the world. However, there are some areas with particularly high background radiation levels. The highest radiation levels are found primarily in Brazil, India and China. In Orissa state, India, for example, average activities of 2500, 220 and 120 $Bqkg^{-1}$ for ^{232}Th, ^{238}U and ^{40}K, respectively, have been reported (Mohanty et al., 2004a, 2004b). At this beach, effective radiation dose rates range between 0.46 and 6.12 $mSvy^{-1}$. In Guarapari, Brazil, gamma radiation dose rates

above 120 $mSvy^{-1}$ have been reported (Radiation Information Network, 2004). In China, radiation dose rates of between 3 and 4 $mSvy^{-1}$ have been reported (Radiation Information Network, 2004).

Table 2.1: Primordial radionuclides with their half-lives and relative abundance/activity (Radiation Information Network, 2004)

Nuclide	Half life	Natural activity (Abundance)
^{235}U	7.04×10^8 y	Abundance: 0.72% of all natural uranium
^{238}U	4.47×10^9 y	Abundance: 99.27% of all natural uranium (0.5 – 4.7 ppm in common rock types)
^{232}Th	1.41×10^{10} y	Abundance: 1.6 to 20 ppm in rock.
^{226}Ra	1.60×10^3 y	Activity: 16 $Bqkg^{-1}$ (in limestone); 48 $Bqkg^{-1}$ (in igneous rock)
^{222}Rn	3.82 days	Noble (inert) Gas; (activity: 28 Bqm^{-3})
^{40}K	1.28×10^9 y	Activity in soil: 37-1100 $Bqkg^{-1}$

Cosmic radiation permeates space, the source being primarily outside of the solar system. The radiation is in many forms, including high-speed heavy particles and high-energy photons and muons. The upper atmosphere interacts with many of the cosmic radiations, resulting in the production of the cosmogenic radionuclides. These radionuclides can have long half-lives, but most have shorter half-lives than the primordial nuclides. Table 2.2 presents some of the common cosmogenic radionuclides (Radiation Information Network, 2004).

Table 2.2: Cosmogenic radionuclides with their half-lives and radioactivity (Radiation Information Network, 2004)

Nuclide	Half life	Source and Natural Activity
^{14}C	5730 y	Source: Cosmic ray interactions; Activity: 220 $Bqkg^{-1}$ in organic matter.
^{3}H	12.3 y	Source: Cosmic ray interactions with N and O; Activity: 1.2×10^{-3} $Bqkg^{-1}$.
^{7}Be	53.3 days	Source: Cosmic ray interactions with N and O; Activity: 0.01 $Bqkg^{-1}$.

Human activities, especially those involving nuclear technologies, e.g., testing of nuclear weapons, nuclear research and energy generation with nuclear reactors, etc., introduce some man-made radionuclides (e.g., ^{137}Cs, and ^{90}Sr) into the environment. The Chernobyl accident of April 26th, 1986, for example, added man-made radionuclides to the environment that resulted in increase in the global average effective radiation dose (UNSCEAR, 2000). However, the collective radiation exposure from all man-made sources is small compared to the natural sources of radiation exposure. A few examples of radionuclides generated from human activities are presented in Table 2.3 (Radiation Information Network, 2004). There are other human activities, such as mining, oil exploration, water works, etc., which are not intended to produce radionuclides but which still result in the enhancement of natural levels of the background radiation.

Table 2.3: Man-made radionuclides and their half-lives and sources (Radiation Information Network, 2004)

Nuclide	Half-life	Source
^{3}H	12.3 y	Weapons testing, fission reactors, and nuclear weapons manufacturing.
^{131}I	8.04 days	Weapons testing and fission reactors; Used in medical treatment of thyroid problems.
^{129}I	1.57×10^{7} y	Weapons testing and fission reactors.
^{137}Cs	30.17 y	Weapons testing and fission reactors
^{90}Sr	28. 78 y	Weapons testing and fission reactors.
^{239}Pu	2.41×10^{4} y	Produced by neutron bombardment of ^{238}U.

2.2 HUMAN EXPOSURES TO ENVIRONMENTAL RADIOACTIVITY

Exposure of human beings to ionizing radiation from naturally occurring radionuclides is a continuing and inescapable feature of life on earth. For most individuals, this exposure exceeds that from all man-made sources combined. There are two main contributors to natural radiation exposures: high-energy cosmic ray particles incident on the earth's atmosphere and natural radionuclides (terrestrial radiation) that originate in the earth's crust and are present everywhere in the environment, including the human body itself. Cosmic radiation increases with altitude (ARPANSA, 2004). Terrestrial radiation comes from naturally occurring radionuclides, mainly from ^{40}K and ^{87}Rb and from ^{238}U and ^{232}Th and their decay products. On average, two thirds of the radiation dose people receive comes from terrestrial sources (ARPANSA, 2004). Most of this dose is from radon gas, a decay product of both uranium and thorium decay series (see appendices 2 and 3, respectively). Radon emanates from the soil and tends to accumulate in buildings,

contributing a high proportion of background radiation dose (ARPANSA, 2006). Both external and internal exposures to humans arise from these sources of radiation.

Terrestrial radiation dose levels are related to the types of rock and place from which the soils originate. Therefore, the natural environmental radiation mainly depends on both geological and geographical conditions. Higher radiation levels are associated with igneous rocks such as granite, and lower levels with sedimentary rocks. There are exceptions, however, as some shale and phosphate rocks have been reported to have relatively high content of natural radionuclides and therefore natural radioactivity (Tzortzis et al., 2003; UNSCEAR, 1993; Zaman et al., 1993). The process of nucleosynthesis in stars forms primordial radionuclides. Only those radionuclides like ^{40}K, ^{238}U and ^{232}Th, with half-lives comparable to the age of the earth, and their radioactive decay products, can still be found today on earth.

2.3 BIOLOGICAL EFFECTS OF RADIOACTIVITY

When radiation is absorbed in the body it causes chemical reactions, which can alter the normal functions of the body. At high doses (i.e., above 1 Sv), radiation can cause massive cell death, organ damage and possibly death to the exposed individual (ICRP, 1991). At low doses (i.e., less than 50 mSv) the situation is more complex and unpredictable (ARPANSA, 2004).

The effects of radiation can be divided into two groups: somatic and genetic effects. Somatic effects affect only the person exposed to radiation while genetic effects affect the offspring of the person exposed to radiation because of damage to the germ cells in the reproductive organs.

The human body is made up of different cells, for example brain cells, muscle cells, blood cells, etc. Genes within a cell determine how the cell functions. If damage occurs to the genes, then it becomes possible for a cancer to occur. This is because the cell loses the ability to control the rate at which it reproduces. Radiation can cause this effect and at low doses it is the only known health effect. This type of event is very unlikely to occur, and an estimate of its frequency of occurrence is only obtained by measuring the effect at higher doses and then calculating the probability at low doses. A dose of 1 mSv corresponds to a chance of 6 in 100,000 of contracting cancer (Jelfs, 1992). If the damage occurs in the testes or ovaries then hereditary effects in descendants may become apparent. No first generation hereditary effects were observed amongst Hiroshima survivors.

Radiation effects can also be divided into stochastic and deterministic (or non-stochastic) effects. Stochastic effects are such that the probability of the effect occurring depends on the dose received, i.e., the higher the dose received the higher the risk of the effect occurring, and vice versa. Development of cancer is the most obvious stochastic effect. Deterministic or non-stochastic effects occur only after a certain radiation dose has been received and the severity of the effect depends on the dose received. Thus deterministic effects have a dose threshold below which they cannot occur. Deterministic effects include development of cataracts, sterility in men, and death.

Because it is not possible to sense the presence of ionizing radiation, one can easily be exposed to a lethal dose of radiation and still not be aware of it until after the event, as happened with early radiation workers. International community concern about the effects of ionizing radiation led to the formation of the International Commission on

Radiological Protection (ICRP) in 1928. The commission has since brought together all the available information on effects of ionizing radiation and recommended dose limits and good working practices in order to minimize the risks from working with ionizing radiation. Based on many studies the ICRP recommends a risk factor of 2 congenital abnormalities per thousand per sievert (Sv) effective dose. This means that a dose of 1 mSv to a large population will produce two (2) cases of severe hereditary effects per million births (UNEP, 1985). This figure is low compared with the normal incidence of severe congenital abnormalities, which incidence is 23,000 per million births (Czeizel et al., 1988).

In areas of high natural background radiation, an increased frequency of chromosome aberrations has been noted repeatedly (Radiation Information Network, 2004). The increases are consistent with those seen in radiation workers and in persons exposed at high radiation dose levels, although the magnitudes of the increases are somewhat higher than predicted. However, no increase in the frequency of cancer cases is noted for most places of high natural background radiation.

In an effort to minimize radiation exposure to members of the public and radiation workers, the ICRP has set limits on exposure to ionizing radiation (Table 2.4). These limits exclude exposure due to background and medical radiation. It is worthwhile to note that exposure to the dose limit is not considered acceptable, and all doses should be kept As Low As Reasonably Achievable (ALARA).

Table 2.4: Annual radiation dose limits recommended by the ICRP (ICRP, 1991)

Population group	Annual effective radiation dose limit ($mSvy^{-1}$)
Members of the public	1
Non-classified workers	15
Classified workers	
Whole body	20
Feet	500
Eyes	150
Hands	500

2.4 ENVIRONMENTAL RADIOACTIVITY STUDIES IN KENYA

There are no nuclear reactors in Kenya but traces of radionuclides from effluents of nuclear reactors in other parts of the world have been reported in Kenya (Hashim et al., 2004). Studies carried out in Kenya have shown that natural radioactivity is due to the primordial radionuclides: ^{238}U, ^{232}Th and ^{40}K (Hashim et al., 2004; Mustapha et al., 2000). Hashim et al., (2004) reported specific radioactivity of ^{238}U, ^{232}Th and ^{40}K in sediments along the Kenyan coastline to be 11.9-22.8 (18.7±2.3), 10.8-26.2 (18.7±3.1) and 206.1-519.2 (401.7±30.9) $Bqkg^{-1}$, respectively. These values are comparable to those reported in other parts of the world (Narayana et al., 2000; Tzortzis et al., 2003, 2004; Tzortzis and Tsertos, 2004) but they are lower than the worldwide averages of 30 and 35 $Bqkg^{-1}$, for ^{232}Th and ^{238}U, respectively (UNSCEAR, 2000).

The population-bias average effective dose rate from natural sources of radiation in Kenya has been estimated to be 3.9 $mSvy^{-1}$ (Mustapha et al., 2000). Mrima hill in the south coast of Kenya has been identified in one study as an area of high background radiation, the effective dose rate ranging from 13.7-106.7 $mSvy^{-1}$ (Patel, 1991), which

is much higher than the normal background radiation of 0.46 $mSvy^{-1}$ (UNSCEAR, 1993). The current study was a screening investigation intended to determine the radioactivity concentrations of the naturally occurring radionuclides in the surface soils around the proposed titanium mining sites in Kwale district of Kenya.

Chapter 3

Theoretical Background of Gamma-Ray spectrometry

3.1 EMISSION OF GAMMA RAYS BY RADIOACTIVE NUCLEI

Most alpha (α) and beta (β) decays, and in fact most nuclear reactions as well, leave the final nucleus in an excited state. These excited states decay rapidly to the ground state through the emission of one or more gamma rays, which are photons of electromagnetic radiation like x-rays or visible light. Gamma rays have energies in the range of 0.1 to 10 MeV, and the corresponding wavelengths are shorter than those of the other types of electromagnetic radiations.

Gamma radiation is due to electromagnetic effects arising out of changes in charge and current distributions in the nucleus. Gamma emission may be accompanied or even replaced by internal conversion due to electromagnetic interactions between the nucleus and extranuclear electrons. Internal conversion results in emission of an electron with kinetic energy equal to the difference between the energy of nuclear transition and the binding energy of the electron. Internal conversion leaves an atom with a vacancy in one of the shells, which is then filled by an electron from the next higher shell. The subsequent atomic rearrangement process may result in emission of characteristic x-rays and in internal photoelectric effects with emission of more electrons from M and L shells.

3.2 INTERACTION OF GAMMA RADIATION WITH MATTER

Charged particles dissipate their energy continuously in a series of many ionizations and excitations. However, the interaction of a gamma ray with matter is a single-event

process that leads to complete absorption or scattering. Gamma rays interact with matter in any of these three ways: (1) Photoelectric Effect, (2) Compton Effect, or (3) Pair Production. These modes of interaction of matter and radiation play important roles in radiation detection and measurement.

3.2.1 Photoelectric Effect

At low photon energies (i.e., below 100 keV), photoelectric effect is the predominant mode of interaction of gamma rays with matter. A photon gives up all its energy to a bound electron, which may then become energetic enough to leave the atom. This is illustrated in Figure 3.1 (Knoll, 1989).

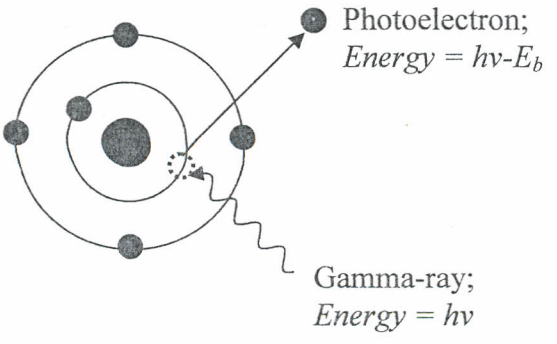

Fig. 3.1: Photoelectric emission of an electron

The kinetic energy, T_e, of the released electron is the difference between the photon energy, hv, and the binding energy of the electron, E_b as expressed in equation 3.1 (Knoll, 1989).

$$T_e = hv - E_b \qquad (3.1)$$

Total absorption of a photon only occurs when an electron is initially at rest so that a third body, the nucleus, conserves momentum (Adams and Dams, 1970).

Photoelectric effect takes place mainly between the inner K- and L- shell electrons. Photoelectric effect is enhanced in absorber materials of high atomic numbers, Z, as shown by the approximation of interaction cross section, τ, in equation 3.2 (Knoll, 1989).

$$\tau = Constant\ x\ \frac{Z^n}{E^{3.5}} \qquad (3.2)$$

where E is the photon energy and the exponent n varies between 4 and 5 over the gamma-ray energy of interest.

3.2.2 Compton Effect

A photon may also be scattered by an atomic or individual electron in a new direction, θ, with or without loss of energy. At photon energies that are very high compared to the binding energies of the electrons, photons are scattered as if the electrons were free and at rest. This process is called the Compton Effect and is dominant at photon energies in the range of 0.6 to 4.0 MeV. The electron that scatters a photon is known as a recoil electron. Figure 3.2 illustrates Compton scattering of a gamma photon.

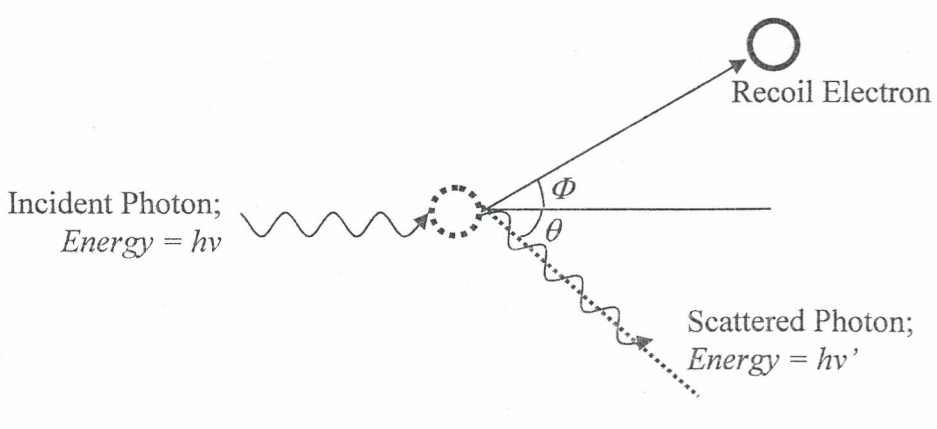

Fig. 3.2: Compton scattering of a Gamma photon (Knoll, 1989)

Using the laws of conservation of energy and momentum, the energy of the scattered photon, hv', is given by (Knoll, 1989)

$$hv' = \frac{hv}{1 + \frac{hv}{m_0c^2}(1-\cos\theta)} \qquad (3.3)$$

where m_0c^2 = 0.511 MeV is the rest mass energy of the electron. The total Compton interaction cross section, σ, is (Knoll, 1989):

$$\sigma = \frac{Z}{E} \qquad (3.4)$$

which increases linearly with the atomic number, Z, of the absorber material.

3.2.3 Pair Production

When photon energy exceeds 1.022 MeV, pair production becomes possible. In this process, an electron pair is created in the coulomb field of a charged particle (Adams et al., 1970). The total kinetic energy of the pair of particles equals the difference between photon energy and the rest mass energy of the particles formed (rest mass energy of the particles = $2m_0c^2$ = 1.022 MeV). Figure 3.3 (Knoll, 1989) illustrates pair production.

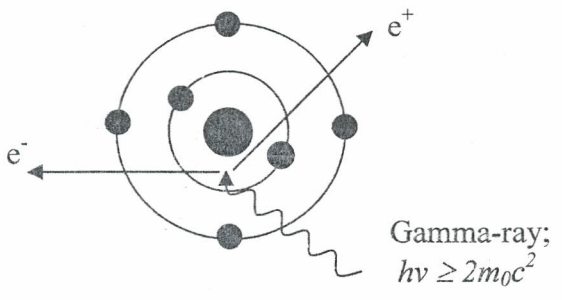

Fig. 3.3: The process of Pair Production

The probability of pair production, k, varies approximately as the square of the atomic number, Z, of the absorber material (Knoll, 1989),

$$k \propto Z^2 \qquad (3.5).$$

3.3 PRINCIPLES OF GAMMA-RAY SPECTROMETRY

All nuclear radiation detection is based on the principles of interaction of radiation with matter. Radiation causes excitation or ionization of atoms in the detector material by the passage of charged particles. Electromagnetic radiation gives rise to energetic electrons by Photoelectric Effect, Compton Effect or Pair Production. These electrons are then detected like other charged particles. In gamma-ray spectrometry, gamma radiation detectors (e.g., high-purity germanium (HpGe) or lithium-drifted sodium iodide, NaI(Tl)) are used to obtain information about energies and intensities of the gamma radiation.

Gamma-ray spectrometry is an analytical method in which radionuclides are identified and quantified based on the gamma rays they emit (IAEA, 1989). The method allows the radionuclides to be measured directly in the original sample without the need for chemical pre-treatment. The form in which the sample is presented to the gamma-ray detector depends on sample type, available equipment, composition of radionuclides and their levels of activity. Some standard sample containers for gamma-ray spectrometry include nylon planchets, aluminium cans and moulded Marinelli beakers. Measuring time in gamma-ray spectrometry varies according to sample type, required detection limits, detection efficiency and nature of the radionuclides of interest.

Determination of identity of a radionuclide depends on inspection of a sample's gamma-ray spectrum (Appendix 4). Identification is done by determination of an unknown radionuclide's characteristic gamma radiation. The degree of confidence of identification directly depends on the precision of measurement of gamma-ray energy. Towards this end, accurate energy calibration of the detector is important. Energy calibration is achieved by use of radionuclide standards (e.g., ^{241}Am, ^{137}Cs and ^{60}Co) with known characteristic gamma-ray energies. The basic equation for radioactivity (in Bqkg^{-1}) calculation is (Mustapha, et al., 2000):

$$A = \frac{N_p}{b.\varepsilon(E_i).m} \qquad (3.6)$$

where A is radioactivity concentration, N_p is net peak area or net intensity of the gamma line in counts per second, b is emission transition probability or branching ratio of the gamma rays during the nuclear de-excitation process, $\varepsilon(E_i)$ is detection efficiency of energy E_i, and m is the mass of the sample in kg.

Alternatively, the radioactivity concentration can be calculated using the method of comparison expressed as equation 3.7 below.

$$\frac{A_{is}\,M_s}{I_{is}} = \frac{A_{iR}M_R}{I_{iR}} \qquad (3.7)$$

where A_{is} = current radioactivity concentration of radionuclide i in the sample, M_s = mass of the sample, I_{is} = intensity or net counts per second (count rate) of radionuclide i in the sample, A_{iR} = current radioactivity concentration of radionuclide i in the

reference sample, M_R = mass of the reference sample, I_{iR} = intensity or net counts per second (count rate) of radionuclide i in the reference material.

The advantage of this method is that it eliminates the need for efficiency calibration at various gamma energies when the matrix of the reference material used is similar to that of the sample analyzed.

3.4 RADIATION DOSE FROM TERRESTRIAL EXPOSURE

Assuming that naturally occurring radioactive nuclides are uniformly distributed in the ground, absorbed radiation dose rates in air at 1 metre above the ground surface are evaluated using the expression below (Kohshi et al., 2001):

$$D = A_U C_U + A_{Th} C_{Th} + A_K C_K \qquad (3.8)$$

where D is absorbed radiation dose rate in $nGyh^{-1}$, A_U, A_{Th} and A_K are the radioactivity concentrations of ^{238}U, ^{232}Th and ^{40}K, respectively in $Bqkg^{-1}$ and C_U, C_{Th} and C_K are the radiation dose conversion factors for ^{238}U, ^{232}Th and ^{40}K, respectively in $nGyh^{-1}$ per $Bqkg^{-1}$. The conversion factors in this equation take into account the attenuation of gamma radiation as it penetrates through the soil.

The radiation dose rate conversion factors used in this study are 0.5281, 0.3892 and 0.0386 $nGyh^{-1}$ per $Bqkg^{-1}$ for ^{232}Th series, ^{238}U series and ^{40}K, respectively. These factors were multiplied by the measured radioactivity concentrations in order to obtain the absorbed radiation dose rate in air due to the entire series. Using this calculation, the absorbed radiation dose rate obtained for ^{232}Th and ^{238}U series is the average for the different dose rates for the different nuclides belonging to each series. For ^{40}K, the radiation dose rate conversion factor is simply the value that is multiplied

by the measured radioactivity concentration at the energy of 1460 keV, in order to deduce the dose rate due to ^{40}K.

In order to make a rough estimate of the annual effective dose outdoors, one has to take into account the conversion coefficient from absorbed dose in air to effective dose and the outdoor occupancy factor. The effective radiation dose rate outdoors in units of μSv per year (μSvy^{-1}) is calculated by the following formula (Tzortzis et al., 2003):

$$D_E = D X C_c \qquad (3.9)$$

where D_E is the effective radiation dose rate in μSvy^{-1}, D is the absorbed radiation dose rate in $nGyh^{-1}$ and C_c is the conversion coefficient in μSvy^{-1} per $nGyh^{-1}$ given by equation 3.10:

C_c = 24 hours per day x 365.25 days per year x 0.4 (occupancy factor) x 0.7 $SvGy^{-1}$ (conversion coefficient) x 10^{-3} = 2.46 μSvy^{-1} per $nGyh^{-1}$ (3.10)

Chapter 4

Materials and Methods

4.1 SAMPLING AND SAMPLE PREPARATION

Samples of surface soil were randomly collected from areas around Nguluku and Maumba villages (Kwale South and Kwale Central dunes, respectively), which are the locations of the proposed mining sites (Figure 4.1a). The sampling area was approximately 15-20 km^2, over a length approximately 10 km. The distance between neighboring sampling points was approximately 500 metres. At each sampling point, approximately 30 cm by 30 cm in size, debris of dead leaves and organisms were first removed, and then the surface soil dug up from a depth of 5-10 cm was thoroughly mixed before three samples, each of volume about 1000 cm^3, were collected. The samples were then sealed in clean and dry polythene bags to avoid cross contamination and labeled appropriately with sampling point name and number, e.g., KTM1 which stands for Kwale Titanium Mine sampling point number 1. Altogether 78 samples were collected from 26 sampling points. The samples were collected and analyzed according to the scheme in Figure 4.1b, which shows that three replicate samples were collected from each of the 26 sampling points and each sample was then tested three times for radioactivity.

In the laboratory, the samples were oven-dried overnight, ground and sieved through 0.5 mm mesh to homogenize the soil, sealed in 450 ml Marinelli beakers, dry-weighed and stored for a minimum of 4 weeks before counting in order to allow the in-growth of radon gas so as to achieve secular equilibrium between ^{226}Ra and its gamma emitting progenies following loss of radon gas during sample preparation.

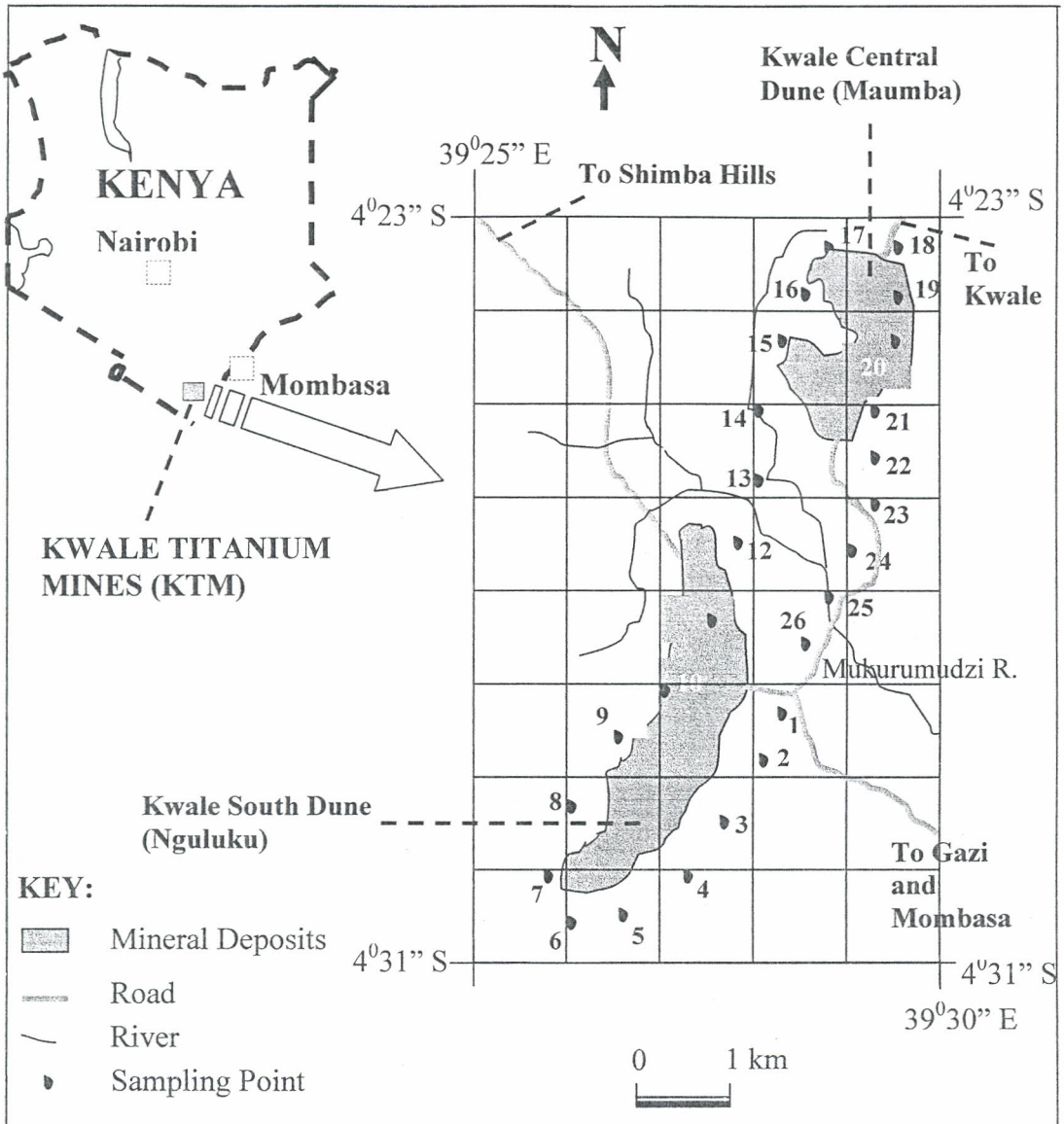

Fig 4.1a: Sampling map and profile

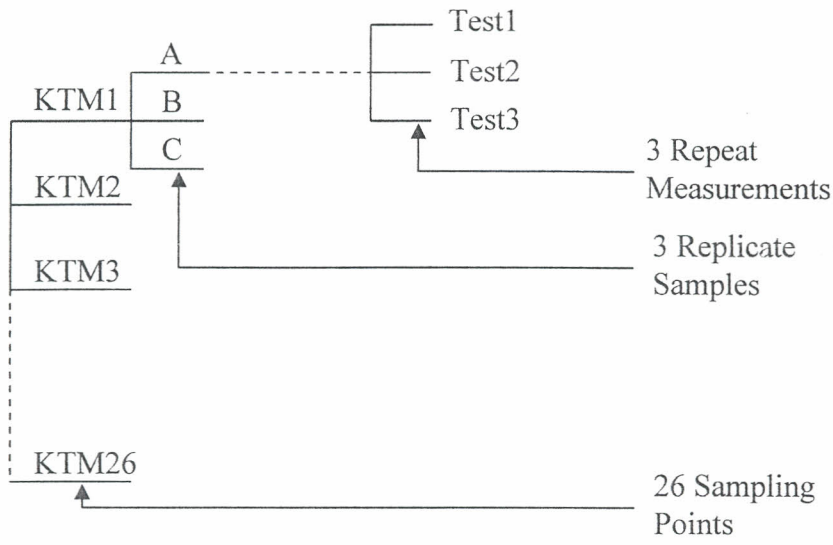

Fig 4.1b: Sampling and sample analysis scheme

4.2 THE EXPERIMENTAL PROCEDURE

4.2.1 Experimental Gamma-Ray Spectrometry System

The 78 soil samples from the mining area were prepared and analysed at the Institute of Nuclear Science and Technology at the University of Nairobi. A stand-alone high-resolution spectroscopic system was used for the measurement of the energy spectrum of the emitted gamma rays in the energy range between 50 and 3000 keV. The system consisted of a high-purity germanium (HpGe) detector (coaxial cylinder of 55 mm in diameter and 73 mm in length) with an efficiency of 20-30%, relative to a 3"x 3" NaI(Tl) scintillator at the 1.33 MeV gamma line of ^{60}Co. The measured energy resolution of the detector was 2.1 keV at the same gamma line (i.e., 1.33 MeV gamma line of ^{60}Co). The detector was mounted on a cryostat which was dipped into a 30 litre Dewar, filled with liquid nitrogen.

Experimental arrangement for spectrometer included the high-voltage bias supply (1200 V) and signal processing electronics. The latter included a main (linear) amplifier and an Oxford PCA3 multi-channel analyser (MCA) with IAEA-GANAAS (IAEA, 1991) PC-based software for data acquisition, storage and display of the acquired gamma spectra. The detector was surrounded by a cylindrical lead shield of thickness 12 cm that provided an efficient suppression of background gamma radiation present in the laboratory environment. A schematic diagram of the HpGe detection system is given in Figure 4.2.

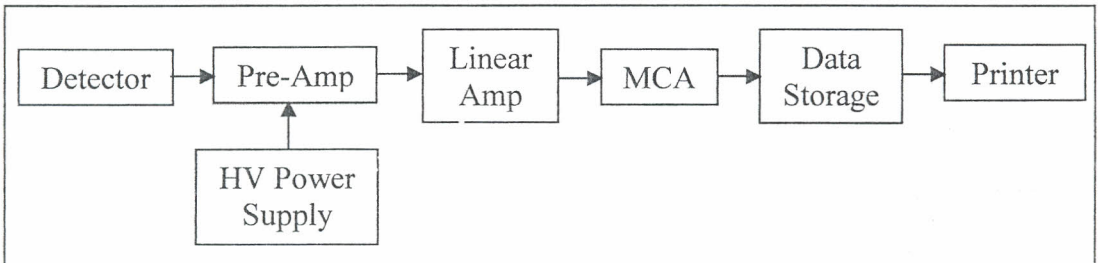

Fig. 4.2: Schematic diagram of HpGe detection system (IAEA, 1989)

4.2.2 Energy Calibration of the Spectrometer System

Identification of radionuclides present in a sample is based on matching the energies of the principal gamma rays in a sample's spectrum to energies of gamma rays in a standard reference sample. Accurate energy calibration is necessary for the detector to be able to assign correct energies for each full energy peak (FEP) in a spectrum (IAEA, 1989; Adams and Dams, 1970). Calibration involves establishment of a channel number of the multi-channel analyser (MCA) in relation to gamma-ray energy.

Over a wide range of gamma-ray energies, it is adequate to express the relationship between the photopeak energy (E) and the channel number as a linear function (IAEA, 1989):

$$E = constant\ X\ Channel\ number + E_0 \qquad (4.1)$$

In this study, energy calibration and evaluation of energy resolution were done using the multi-nuclide SRM-1 standard reference material obtained from the IAEA. The calibration source was counted for long periods in order to obtain well-defined photopeaks (Appendix 1). The gamma lines used for calibration were 59.54 keV (^{241}Am), 661.66 keV (^{137}Cs), and 1173.24 keV and 1332.5 keV (^{60}Co). The energy resolution (full width at half-maximum or FWHM) achieved by the spectrometer was 2.1 keV at the 1.33 MeV reference gamma line of ^{60}Co.

4.2.3 Sample Counting

The samples were counted on the shielded HpGe detector for long periods, ranging from 30,000 to 60,000 seconds. For each sample, three measurements were made (see the sampling and sample analysis scheme, Figure 4.1b). Prior to the samples' measurement, the environmental gamma background at the laboratory site was determined with a Marinelli beaker full of distilled water under identical measurement conditions. This background was later subtracted from the measured gamma-ray spectra of each sample.

Each gamma-ray spectrum obtained was analyzed by a dedicated GANAAS computer software (IAEA, 1991), which performed a simultaneous fit to all the significant photopeaks appearing in the spectrum, to provide reports with summaries on information that include centroid energy, net counts, background counts, intensity

(count rate) and width (FWHM) of identified and unidentified peaks in the spectrum (Appendix 4). The naturally occurring radionuclides (^{232}Th, ^{238}U and ^{40}K) were identified and evaluated for radioactivity by using the spectra of RGTh-1, RGU-1 and RGK-1 standard reference materials, respectively. These reference materials, obtained from the IAEA, were selected for this analysis because they are mixtures of geological materials and are, therefore, suitable for analysis of other geological materials like soil.

4.2.4 Calculation of Radioactivity

The radioactivity concentration of ^{232}Th was estimated using the average of the radioactivity concentrations of ^{212}Pb (at 238 keV), ^{208}Tl (at 583 keV) and ^{228}Ac (at 911 keV) while the radioactivity concentration of ^{226}Ra was estimated from the average of the radioactivity concentrations of ^{214}Pb (at 295 keV and 352 keV) and ^{214}Bi (at 609 keV). Radioactivity concentration of ^{40}K was determined directly using its 1460 keV gamma line. Radioactivity concentration of each radionuclide in each sample was determined using the method of radioactivity comparison with standard reference material earlier described in section 3.3.

4.2.5 Detection Limits

The detection limit, L_{Di} of a radionuclide i in a spectrum was evaluated according to the following expression (Derbertin and Helmer, 1988):

$$L_{Di} = 5.4 + 3.32(N_{bi})^{0.5} \qquad (4.2)$$

where N_{bi} is the background count of nuclide i in the laboratory environment.

4.3 GAMMA RADIATION DOSE RATES

The likely absorbed radiation dose rate in air at 1 metre above the ground surface was evaluated according to expression 3.8 (see section 3.4). The absorbed gamma radiation dose rate in air was mainly determined from the radioactivity concentrations ($Bqkg^{-1}$) of ^{232}Th series, ^{238}U series and ^{40}K, and their respective dose conversion factors ($nGyh^{-1}$ per $Bqkq^{-1}$). In the UNSCEAR recent reports (UNSCEAR, 1993; 2000), the Committee used 0.7 $SvGy^{-1}$ for the conversion coefficient from absorbed dose in air to effective dose received by adults, and 0.2 for the outdoor occupancy factor. In this study, the same value of conversion coefficient (0.7 $SvGy^{-1}$) was used but an average value of 0.4 was used for the occupancy factor because of geographical, climatic and social factors, which allow residents of the proposed mining areas to stay outdoors for longer periods than the average global period of outdoor occupancy. Kwale district and Kenya in general, lies within the tropics where daylights are longer and daily temperatures are higher than in many other areas of the world. Also, the residents of the area of study generally spend long periods of time socializing outdoors. Using these values, effective dose rate outdoors in units of μSvy^{-1} was calculated from equation 3.9.

Chapter 5

Results and Discussion

5.1 QUALITY CONTROL AND ASSURANCE

To ensure reproducibility of results, the stability of the spectrometer was monitored regularly by measuring the energy resolution of the detector prior to each sample counting. This was done throughout the period of study and an average energy resolution of 2.1±0.3 keV was obtained at the 1.33 MeV reference gamma line of ^{60}Co.

Background radioactivity in the laboratory environment was measured under identical conditions using distilled water in a Marinelli beaker. This background radioactivity was measured prior to each sample measurement and was later subtracted from the sample spectra.

Also, detection limits of the detector for ^{232}Th, ^{238}U (or ^{226}Ra) and ^{40}K were determined. The average values of these detection limits are listed in Table 5.1.

Table 5.1: Mean detection limits of the HpGe detector

Radionuclide	Detection limit, L_D, ($Bqkg^{-1}$)
^{232}Th	6.23±0.087
^{238}U	5.49±0.034
^{40}K	5.92±0.006

The standard reference materials (RGTh-1, RGU-1, and RGK-1) were analyzed as unknown samples and their respective radioactivity levels determined. These measured values were then compared with the certified values of these standards to

determine the accuracy and reliability of measurements. The radioactivity levels of ^{232}Th, ^{238}U and ^{40}K obtained for the standard reference materials are presented in Table 5.2.

Table 5.2: Measured and Certified values of radioactivity ($Bqkg^{-1}$) of the reference materials RGTh-1, RGU-1, and RGK-1 (IAEA, 1987)

Reference Material	Measured Radioactivity, (A_m)	Certified Radioactivity, (A_c)	Deviation, D (%)
RGTh-1 (^{232}Th)	3026±251	3280	7.7
RGU-1 (^{238}U)	4512±379	4910	8.1
RGK-1 (^{40}K)	11632±1203	13370	8.5

A plot of the measured values against the certified values of radioactivity for these standard materials is shown in Figure 5.1 below. The plot shows that the measured values are in good agreement with the certified values. (The correlation coefficient = 0.999). The relative deviations of the measured activities from the certified activities are between 7.7% and 8.5%. Representing the measured values of radioactivity of the standard reference material (SRM) with y and the certified values with x, the equation of the line of best fit for the values in table 5.2 is $y = 0.85x + 287$, which is the equation of a straight line. These measurements of the reference activities suggest that the accuracy of the measurements of radioactivity levels in the soil samples is acceptable and reliable.

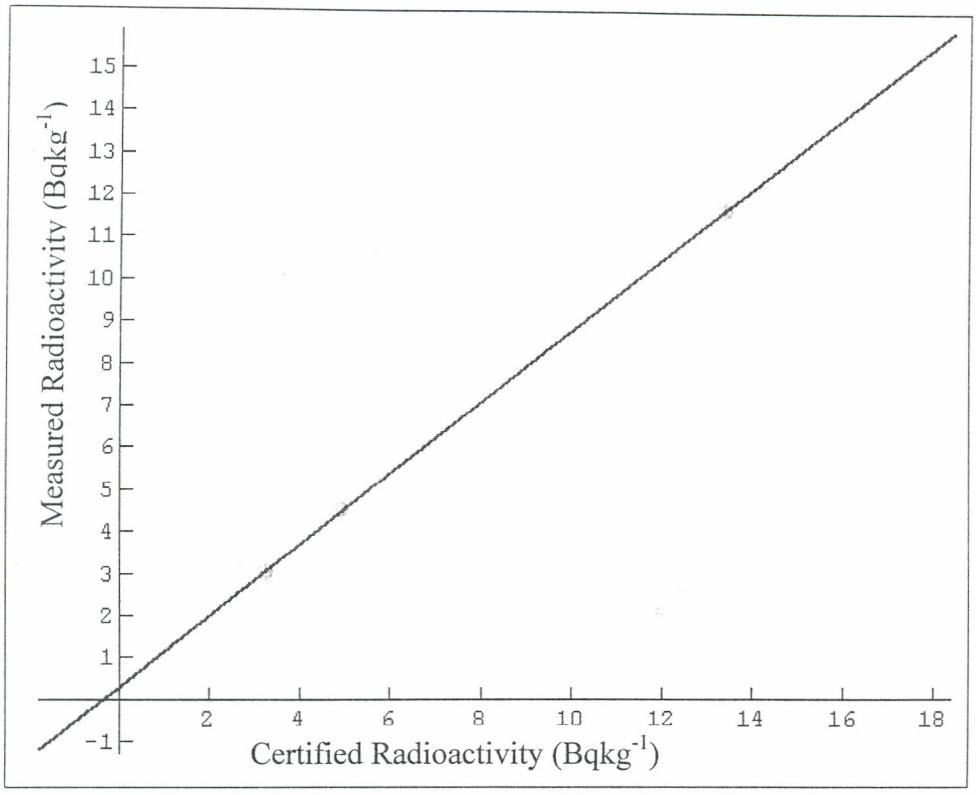

Fig. 5.1: Correlation of measured values with certified values of radioactivity of reference materials

5.2 RADIOACTIVITY CONCENTRATIONS OF RADIONUCLIDES

A typical gamma-ray spectrum of the tested soil samples is shown in Figure 5.2 below. As can be seen from the spectral data, only naturally occurring radionuclides were observed in the soil samples that were analyzed. This is not unexpected since there are no nuclear industries in Kenya, including in the environment of the study area.

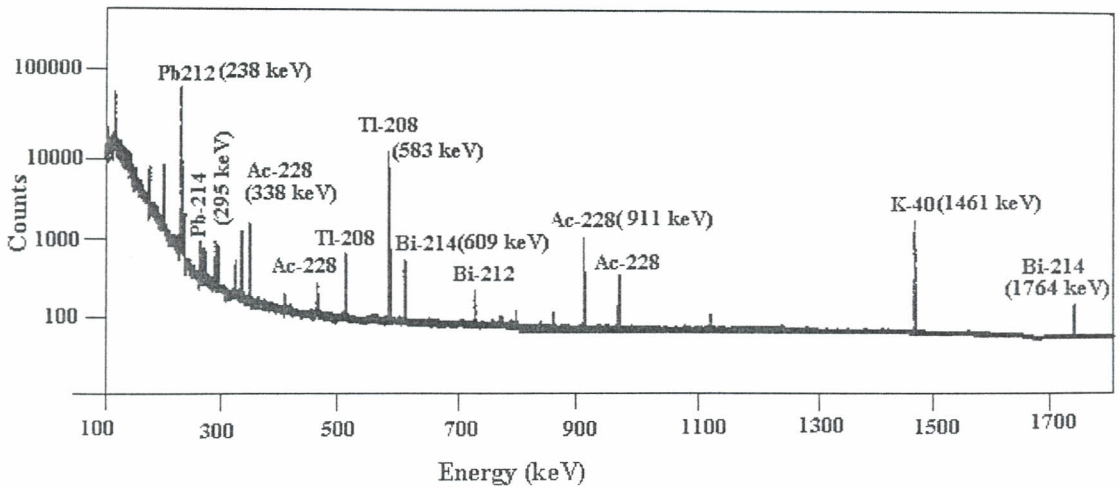

Fig. 5.2: Typical gamma-ray spectrum of a soil sample

Tables 5.3a, 5.3b and 5.3c present the values of radioactivity concentrations of ^{232}Th, ^{226}Ra (^{238}U) and ^{40}K in the soil samples that were analyzed. The samples have been named KTM1 through KTM26 e.g., KTM1 means sampling point number 1 (an abbreviation of Kwale Titanium Mines sampling point 1) and A, B, and C are the three replicate samples from the same sampling point. Table 5.4 presents a summary (minimum, maximum and mean) of these radioactivity concentrations for each radionuclide in the soil samples analyzed.

Table 5.3a: Radioactivity concentration ($Bqkg^{-1}$) of ^{232}Th in soil samples

Sampling Site	Sample A	Sample B	Sample C	Mean Value
KTM1	17.2±2.9	17.6±1.5	16.5±3.0	17.1±0.3
KTM2	34.1±3.1	33.2±0.9	33.8±1.9	33.7±0.3
KTM3	7.9±0.6	8.1±1.1	9.2±1.6	8.4±0.4
KTM4	11.1±2.1	10.5±1.4	10.5±1.3	10.7±0.2
KTM5	13.2±1.9	13.8±2.0	16.8±2.2	14.6±1.1
KTM6	42.7±2.3	41.6±3.5	46.5±2.8	43.6±1.5
KTM7	37.8±2.1	41.1±3.8	38.7±3.7	39.2±1.0
KTM8	20.3±2.9	22.6±3.0	20.1±1.9	21.0±0.8
KTM9	39.0±2.5	38.5±3.4	35.6±2.6	37.7±1.1
KTM10	32.9±3.0	33.1±2.8	35.7±1.9	33.9±0.9
KTM11	32.1±2.5	34.8±2.0	31.2±2.5	32.7±1.1
KTM12	40.2±2.1	35.9±3.3	33.7±1.7	36.6±1.9
KTM13	37.7±3.2	38.1±2.7	42.1±3.8	39.3±1.4
KTM14	20.3±3.1	24.6±2.0	20.2±1.9	21.7±1.5
KTM15	30.3±2.0	29.9±3.2	34.6±3.5	31.6±1.5
KTM16	32.1±2.4	32.5±2.7	33.8±3.1	32.8±0.5
KTM17	27.9±3.4	31.4±1.9	28.3±2.0	29.2±1.1
KTM18	19.3±1.0	17.7±2.1	18.5±1.1	18.5±0.5
KTM19	25.7±1.2	27.0±1.6	30.1±2.2	27.6±1.3
KTM20	25.1±2.5	26.1±2.3	27.4±1.9	26.2±0.7
KTM21	21.5±1.8	22.6±2.1	20.1±2.4	21.4±0.7
KTM22	27.2±3.1	29.9±2.5	32.3±2.2	29.8±1.5
KTM23	30.2±1.7	27.1±3.3	27.3±1.9	28.2±1.0
KTM24	32.2±3.0	32.8±2.1	30.7±2.4	31.9±0.6
KTM25	30.1±2.5	28.1±2.5	26.4±3.2	28.2±1.1
KTM26	22.1±1.9	23.0±1.9	19.7±1.8	21.6±1.0

Table 5.3b: Radioactivity concentration ($Bqkg^{-1}$) of ^{226}Ra (^{238}U) in soil samples

Sampling Site	Sample A	Sample B	Sample C	Mean Value
KTM1	13.5±1.0	12.9±1.8	15.9±2.1	14.1±0.9
KTM2	25.5±2.1	28.9±3.1	24.2±2.8	26.2±1.4
KTM3	7.9±0.8	6.3±1.9	8.0±1.9	7.4±0.6
KTM4	8.9±1.2	9.1±1.7	10.8±1.9	9.6±0.6
KTM5	12.7±2.0	13.2±3.4	10.4±2.2	12.1±0.9
KTM6	38.3±2.8	41.2±4.3	42.3±3.8	40.6±1.4
KTM7	31.3±3.9	29.9±2.7	29.1±1.9	30.1±0.6
KTM8	14.4±2.0	15.9±1.0	16.5±2.2	15.6±0.6
KTM9	30.6±2.5	31.0±3.4	33.2±3.3	31.6±0.8
KTM10	25.1±2.7	29.9±2.8	26.0±3.0	27.0±1.5
KTM11	22.1±2.1	20.9±2.8	18.2±1.6	20.4±1.2
KTM12	23.3±1.1	22.4±1.4	22.1±2.0	22.6±0.4
KTM13	33.5±2.2	31.9±3.0	32.7±3.4	32.7±0.5
KTM14	18.3±1.8	16.9±1.0	16.4±2.1	17.2±0.6
KTM15	24.2±2.8	26.7±2.5	25.9±3.0	25.6±0.7
KTM16	22.8±2.2	25.1±2.5	25.0±1.9	24.3±0.8
KTM17	19.0±2.1	17.8±2.0	17.5±1.9	18.1±0.5
KTM18	14.2±0.8	16.3±1.9	16.3±1.8	15.6±0.7
KTM19	20.4±2.7	18.8±2.2	20.5±2.8	19.9±0.6
KTM20	15.0±1.1	13.9±2.3	14.9±1.9	14.6±0.4
KTM21	16.6±2.0	17.9±2.7	17.4±0.9	17.3±0.4
KTM22	22.9±1.2	24.1±2.4	23.5±2.1	23.5±0.3
KTM23	18.3±1.7	16.9±1.9	18.2±3.0	17.8±0.5
KTM24	24.1±2.1	22.2±3.1	23.6±2.4	23.3±0.6
KTM25	19.1±2.5	17.6±3.3	17.9±2.4	18.2±0.5
KTM26	18.3±2.0	17.1±1.1	17.7±1.8	17.7±0.3

Table 5.3c: Radioactivity concentration ($Bqkg^{-1}$) of ^{40}K in soil samples

Sampling Site	Sample A	Sample B	Sample C	Mean Value
KTM1	63.2±5.5	66.1±6.0	67.8±4.0	65.7±1.3
KTM2	76.8±2.7	79.4±7.1	75.7±5.7	77.3±1.1
KTM3	32.0±2.4	29.6±2.8	34.1±3.5	31.9±1.3
KTM4	67.7±6.5	66.6±7.0	60.1±3.7	64.8±2.4
KTM5	45.9±3.8	48.9±4.9	39.0±1.9	44.6±2.9
KTM6	54.1±3.0	57.9±2.5	56.0±5.0	56.0±1.1
KTM7	52.1±2.4	53.2±3.3	56.1±1.9	53.8±1.2
KTM8	67.9±2.0	69.1±3.2	62.5±2.7	66.5±2.0
KTM9	55.3±2.1	50.8±2.6	55.0±4.0	53.7±1.5
KTM10	66.1±6.0	60.9±3.9	66.8±6.4	64.6±1.9
KTM11	73.3±3.1	72.9±5.8	71.3±4.9	72.5±0.6
KTM12	78.9±5.4	75.7±4.6	77.6±4.4	77.4±0.9
KTM13	47.8±4.8	44.6±3.5	49.2±3.3	47.2±1.4
KTM14	77.0±2.9	79.9±4.5	75.9±2.8	77.6±1.2
KTM15	76.1±3.3	79.3±4.5	73.5±4.0	76.3±1.7
KTM16	86.8±5.2	88.1±5.5	89.7±4.5	88.2±0.8
KTM17	85.4±5.8	86.6±6.0	81.2±4.3	84.4±1.6
KTM18	70.7±3.4	72.9±3.9	70.6±4.4	71.4±0.8
KTM19	112.1±3.3	116.7±4.0	113.5±2.2	114.1±1.4
KTM20	95.5±3.4	90.2±4.4	93.6±4.0	93.1±1.6
KTM21	82.2±5.0	79.9±6.1	78.5±4.2	80.2±1.1
KTM22	68.7±2.2	66.4±2.8	63.5±4.1	66.2±1.5
KTM23	75.5±2.2	73.4±5.0	75.2±2.7	74.7±0.7
KTM24	65.5±5.5	66.3±4.3	65.6±3.5	65.8±0.3
KTM25	73.2±3.8	71.9±3.7	70.0±3.0	71.7±0.9
KTM26	67.7±3.9	64.9±2.6	65.7±5.5	66.1±0.8

In the present study, the radioactivity of ^{238}U has been taken to be the same as that of ^{226}Ra, which is a member of the ^{238}U decay series. Therefore, radioactivity values of ^{226}Ra are presented in place of those of ^{238}U. The presentation of values of radioactivity of ^{226}Ra in place of those of ^{238}U is based on the fact that in the ^{238}U decay series, ^{226}Ra is the chief nuclide of environmental interest as it and its progeny produce up to 98% of the radiation from the series.

In tables 5.3a, 5.3b and 5.3c it is shown that radioactivity concentrations ranged between 8.4±0.4 and 43.6±1.5 $Bqkg^{-1}$, with a mean value of 27.6±1.7 $Bqkg^{-1}$ for ^{232}Th, between 7.4±0.6 and 40.6±1.4 $Bqkg^{-1}$ with a mean value of 20.9±1.5 $Bqkg^{-1}$ for ^{226}Ra and between 31.9±1.3 and 114.1±1.4 $Bqkg^{-1}$ with a mean value of 69.5±3.2 $Bqkg^{-1}$ for ^{40}K (Table 5.4).

Table 5.4: Minimum, maximum and mean radioactivity concentrations ($Bqkg^{-1}$) of ^{232}Th, ^{226}Ra and ^{40}K in Soil

Nuclide	Minimum Radioactivity	Maximum Radioactivity	Mean Radioactivity
^{232}Th	8.4±0.4	43.6±1.5	27.6±1.7
^{226}Ra	7.4±0.6	40.6±1.4	20.9±1.5
^{40}K	31.9± 1.3	114.1±1.4	69.5±3.2

The average values of radioactivity of both ^{232}Th and ^{226}Ra in the present study (Table 5.4) are similar to those reported for the sediments along the Kenyan coastline (Hashim et al., 2004) and to the normal global averages (UNSCEAR, 2000). However, the radioactivity of ^{40}K in the present study is lower than that reported in the cited literature. The average radioactivity concentration of ^{40}K in the samples analyzed (69.5±3.2 $Bqkg^{-1}$) was lower than the global average of 400 $Bqkg^{-1}$. Radioactivity concentration of ^{40}K at the Kenyan coast has previously been reported

to be 401.7 $Bqkg^{-1}$ (Hashim et al., 2004). One possible cause of the low level of radioactivity of ^{40}K in the analyzed soil could be leaching of the potassium from upper layers of soil to lower layers, considering the fact that potassium forms soluble salts and the sandy soils analyzed in this study easily permit leaching of dissolved minerals from upper to lower layers of soil.

Figures 5.3a, 5.3b, and 5.3c represent the mean values in Tables 5.3a, 5.3b and 5.3c. In each case, both a bar chart and a normal probability distribution curve are presented for comparison. The measured values differ slightly from normal probability distributions. The values of skewness of the measured values relative to normal probability distributions are -0.40, 0.62 and 0.25 respectively, for ^{232}Th, ^{226}Ra and ^{40}K. The values of kurtosis of these measured values are -0.42, 0.55 and 1.56 respectively, for ^{232}Th, ^{226}Ra and ^{40}K.

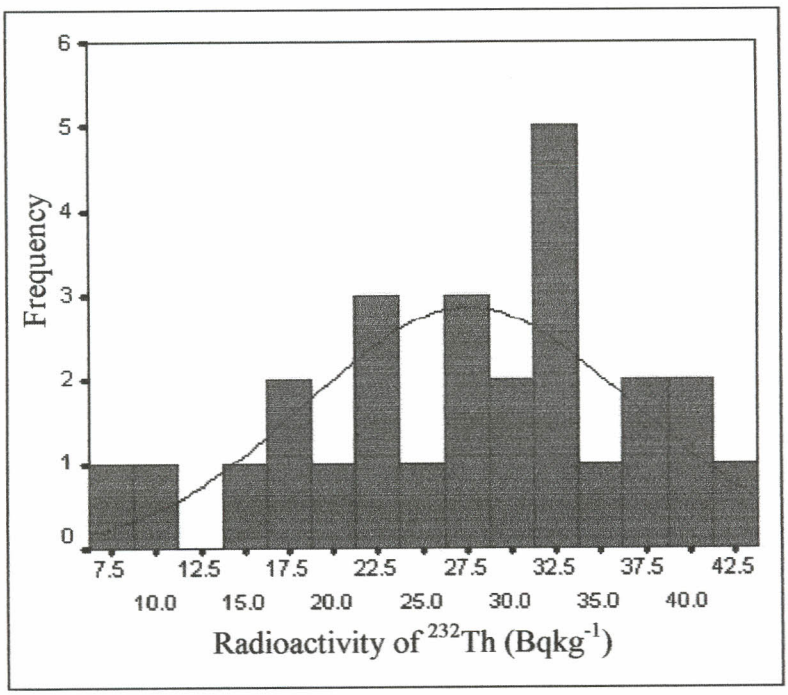

Fig. 5.3a: ^{232}Th radioactivity levels in soil

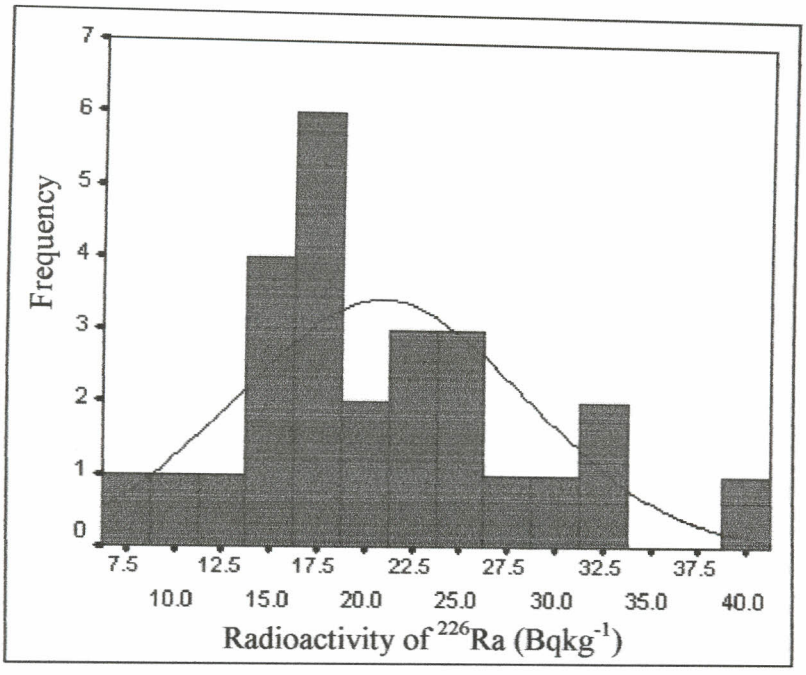

Fig. 5.3b: ^{226}Ra radioactivity levels in soil

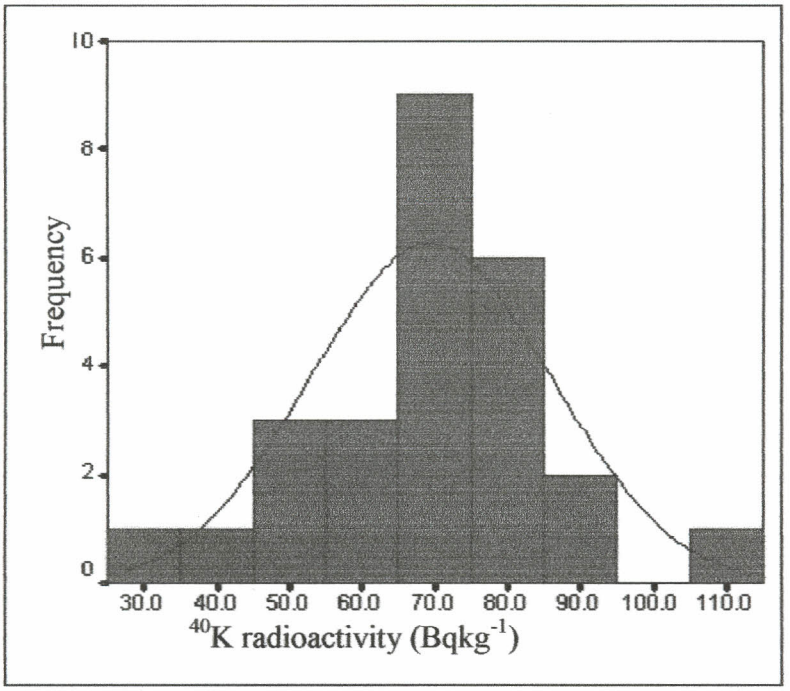

Fig. 5.3c: ^{40}K radioactivity levels in analyzed soil

The sample with the highest value of radioactivity of ^{232}Th also had the highest value of radioactivity of ^{226}Ra. Similarly, the sample with the lowest radioactivity of ^{232}Th

was the one with the lowest radioactivity of ^{226}Ra. This suggests existence of a linear correlation between the values of radioactivity of ^{232}Th and ^{226}Ra in the samples analyzed. The ratios of radioactivity concentrations of ^{232}Th to those of ^{226}Ra (^{238}U) in the soil samples varied between 1.1 and 1.8 with a mean of 1.3±0.01. The radioactivity concentrations of ^{232}Th and ^{226}Ra obtained in this study actually had a strong linear correlation between them (correlation coefficient = 0.93). There was only a weak linear correlation between ^{232}Th and ^{40}K (correlation coefficient = 0.12) and between ^{226}Ra and ^{40}K (correlation coefficient = -0.08). A strong correlation between ^{226}Ra and ^{232}Th radioactivity means that the presence of ^{232}Th in a sample is accompanied by the presence of ^{226}Ra in the same sample. A strong correlation between ^{226}Ra and ^{232}Th is an indication of the presence of significant amounts of monazite and zircon sands in the soil (Mohanty et al., 2004). Monazite is a natural orthophosphate, which can incorporate large quantities of actinides (thorium and uranium) in its crystal structure during formation (Overstreet, 1967; Gramaccioli and Segalstad, 1978; Emden et al., 1997).

A weak linear correlation between ^{232}Th and ^{40}K, and also between ^{226}Ra and ^{40}K, implies that the presence of ^{232}Th (or ^{226}Ra) in a soil may not indicate presence of ^{40}K. The weak correlation between ^{40}K and ^{226}Ra and between ^{40}K and ^{232}Th in the samples also suggests that individual results of ^{40}K and ^{226}Ra or ^{40}K and ^{232}Th are not dependent on each other. Figures 5.4a, 5.4b, and 5.4c show the variations between the radioactivity concentrations of ^{226}Ra and ^{232} Th, those of ^{232}Th and ^{40}K, and those of ^{226}Ra and ^{40}K, respectively.

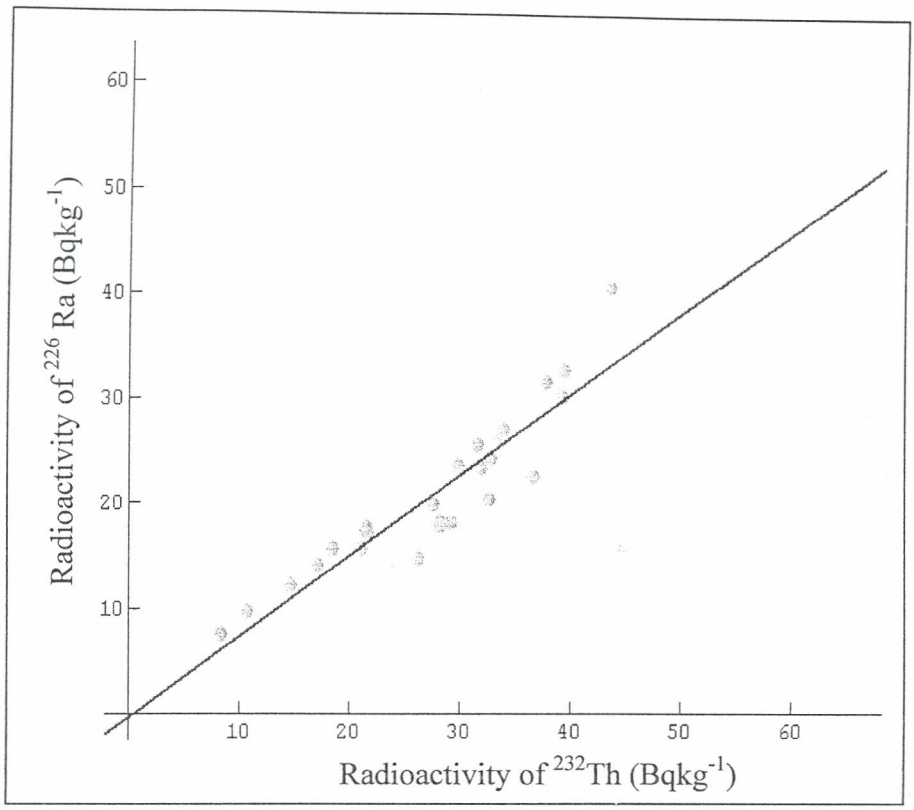

Fig. 5.4a: Variation of radioactivity concentration of ^{232}Th with that of ^{226}Ra

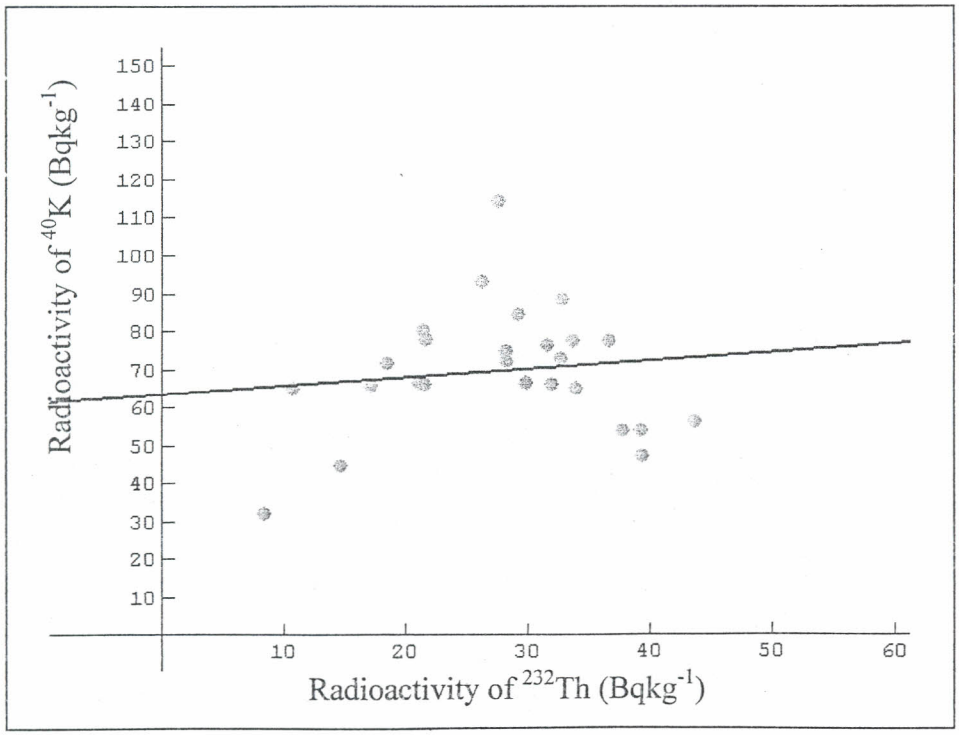

Fig. 5.4b: Variation of radioactivity concentration of ^{232}Th with that of ^{40}K

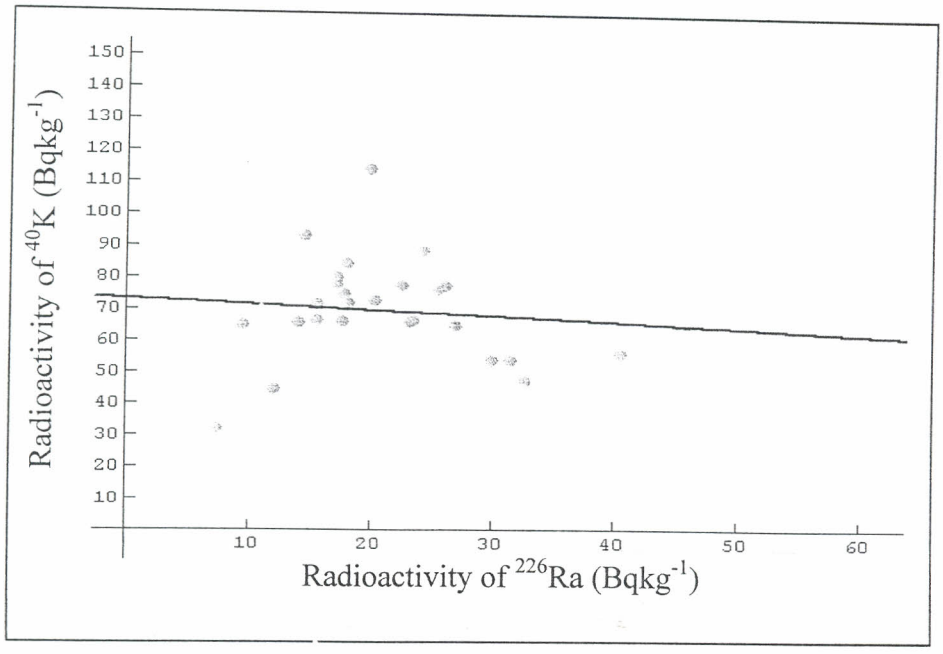

Fig. 5.4c: Correlation of radioactivity concentration of ^{226}Ra with that of ^{40}K

5.3 HUMAN EXPOSURE TO GAMMA RADIATION

The distribution of radionuclides in surface soil was assumed to be uniform. Absorbed dose rates in air outdoors due to ^{232}Th and ^{238}U decay series products and ^{40}K for the soil samples were then calculated from the radioactivity concentrations of the respective nuclides using equation 3.8 in section 3.4.

The values of absorbed gamma radiation dose rate obtained for each of the 26 sampling points are presented in Table 5.5, which also shows corresponding values of effective dose rates. As shown in the table, the values of total absorbed gamma radiation dose rates range between 8.5±0.5 and 36.9±1.1 nGyh^{-1} with a mean of 25.2±1.4 nGyh^{-1}. Corresponding values of total effective gamma radiation dose rates (obtained using equation 3.9) range between 21.0±1.2 and 90.8±2.6 μSvy^{-1} with a mean value of 62.0±3.5 μSvy^{-1} (Table 5.6).

Table 5.5: Absorbed and effective gamma radiation dose rates in soil

Sample	Absorbed dose rate ($nGyh^{-1}$)	Effective dose rate (μSvy^{-1})
KTM1	17.1±0.6	42.0±1.4
KTM2	31.0±0.7	76.2±1.8
KTM3	8.5±0.5	21.0±1.2
KTM4	11.9±0.4	29.2±1.1
KTM5	14.1±1.0	34.8±2.6
KTM6	36.9±1.1	90.8±2.6
KTM7	34.5±0.8	84.9±2.0
KTM8	19.7±0.7	48.5±1.8
KTM9	34.3±0.9	84.3±2.3
KTM10	30.9±1.1	76.0±2.8
KTM11	28.0±1.0	68.9±2.6
KTM12	31.1±1.2	76.5±2.9
KTM13	35.3±1.0	86.8±2.4
KTM14	21.1±1.0	52.0±2.5
KTM15	29.6±1.1	72.8±2.8
KTM16	30.2±0.6	74.3±1.5
KTM17	25.7±0.8	63.3±2.0
KTM18	18.6±0.5	45.7±1.3
KTM19	26.7±1.0	65.7±2.4
KTM20	23.1±0.5	56.9±1.3
KTM21	21.1±0.6	52.0±1.4
KTM22	27.4±1.0	67.5±2.4
KTM23	24.7±0.7	60.8±1.8
KTM24	28.5±0.6	70.0±1.4
KTM25	24.7±0.8	60.9±1.9
KTM26	20.8±0.7	51.3±1.7

Table 5.6: Minimum, maximum and mean absorbed ($nGyh^{-1}$) and effective (μSvy^{-1}) gamma radiation dose rates in the tested soil samples

	Minimum	Maximum	Mean
Absorbed dose rate	8.5±0.5	36.9±1.1	25.2±1.4
Effective dose rate	21.0±1.2	90.8±2.6	62.0±3.5

In terms of individual radionuclides, ^{232}Th seemed to contribute higher average absorbed radiation dose rate (14.6 $nGyh^{-1}$) than ^{226}Ra (8.1$nGyh^{-1}$) and ^{40}K (2.7 $nGyh^{-1}$) as shown in Figure 5.5, which compares the percentage contributions to gamma radiation of these nuclides in the analyzed soil with respective global average contributions. The relative (%) contribution to radiation dose rate by ^{40}K was 11%, while contributions due to radionuclides ^{226}Ra and ^{232}Th and their decay progeny were 32% and 57%, respectively. It is estimated that ^{232}Th contributes 40%, ^{238}U (^{226}Ra) 25% and ^{40}K 35% to global terrestrial radiation (UNSCEAR, 1988). The relative (%) contributions of ^{232}Th and ^{226}Ra to radiation dose rate in this study were higher than their global averages while the relative contribution of ^{40}K to radiation dose rate was lower than its global average value.

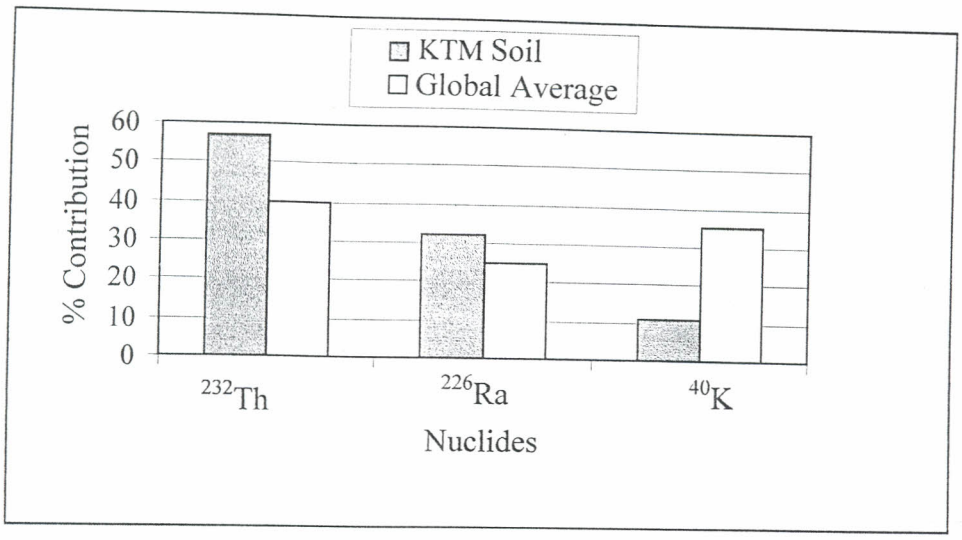

Fig. 5.5: Contributions of ^{226}Ra, ^{232}Th and ^{40}K to gamma radiation dose rate

According to the UNSCEAR reports (1993, 2000), the worldwide average absorbed gamma radiation dose rates range between 8 and 93 $nGyh^{-1}$. The population-weighted values give an average absorbed dose rate in air outdoors from terrestrial gamma radiation of 60 $nGyh^{-1}$, which is higher than that obtained in the present study (25.2±1.4 $nGyh^{-1}$) by a factor of more than two. Based on this comparison, the radiation dose rate from the soil samples around the proposed titanium mines is considered low, presenting little or no radiological risk.

The mean effective radiation dose rate (62.0 μSvy^{-1}) obtained in this study is below the normal global background radiation average of 460 μSvy^{-1} (UNSCEAR, 1993). The values of effective radiation dose rate obtained in this study are in close agreement with those obtained earlier by Hashim et al., (2004) for the Kenyan coastline but they are far below the range 13.7-106.7 $mSvy^{-1}$ reported for the nearby Mrima hill, a monazite mineralized area (Patel, 1991). The values of radiation dose rates obtained in this study are also below the ICRP-recommended limits of exposure of workers and members of the public (ICRP, 1991).

The values of absorbed and effective radiation dose rates in Table 5.5 are represented by the charts in Figures 5.6a and 5.6b. A fitted normal distribution curve indicates that the radiation dose rates are approximately normally distributed.

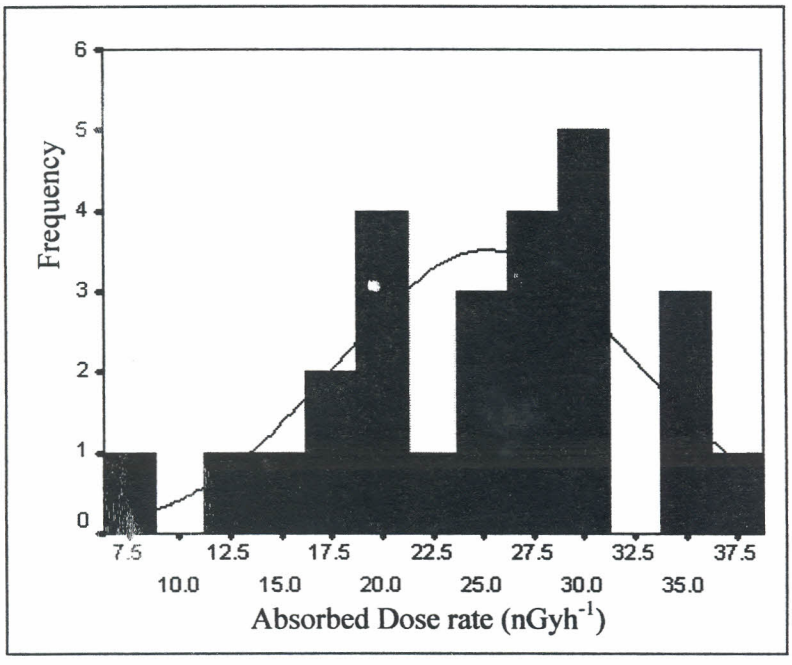

Fig. 5.6a: Distribution of absorbed dose rate ($nGyh^{-1}$) in the analyzed soil samples

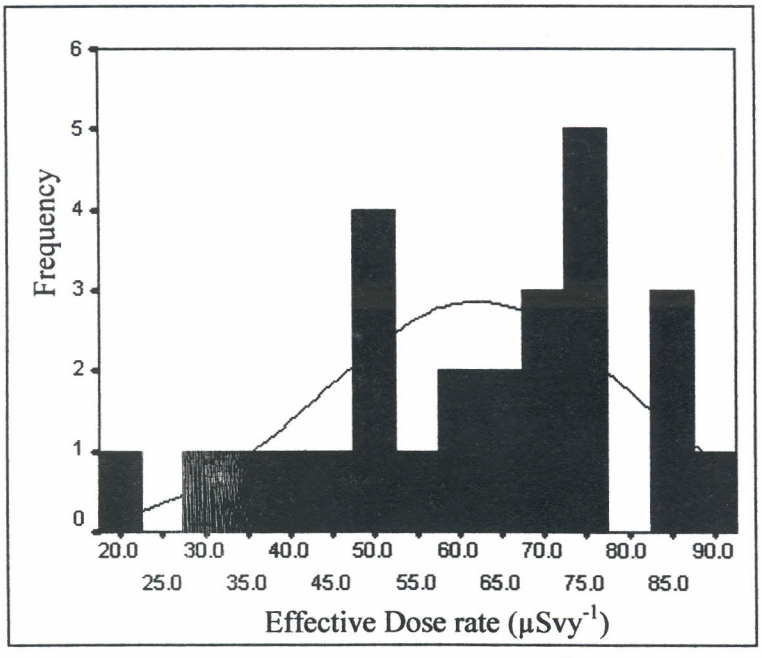

Fig. 5.6b: Distribution of effective dose rate (μSvy^{-1}) in analyzed soil samples

The above effective gamma dose rates, D_E, was used to estimate the annual number, N, of gamma radiation exposure-induced deaths in a population, N_P. A dose-to-risk conversion factor (DRCF) of 6% per sievert (Jelfs, 1992) applied to the mean effective dose rate of 62.0 microsievert per year indicates that in a population, N_P, of 3,000 people (equal to the estimated population of the proposed mining area) exposed to gamma radiation from this soil, the number of likely deaths N, due to cancer caused by this radiation is:

$N = D_E \times DRCF \times N_P$

$N = 62.0 \times 10^{-6}$ sievert x 6% per sievert x 3000 people $\approx$ 0.01 people.

Thus the estimated average number of people likely to die due to exposure to gamma radiation from this soil is negligible. However, this number may vary because the dose-to-risk conversion factor varies with parameters such as sex, age, critical organ and sensitivity to radiation-induced cancer of the individuals exposed to radiation.

Chapter 6

Conclusions and Recommendations

6.1 CONCLUSION

In this study, the radioactivity concentrations of natural radionuclides in surface soil around the proposed titanium mines in Kwale district are reported. Corresponding gamma radiation dose rates have been calculated from these activities and are also reported.

For the soil samples that were investigated, the levels of radioactivity concentrations vary between 8.4±0.4 and 43.6±1.5 $Bqkg^{-1}$ with a mean of 27.6±1.7 $Bqkg^{-1}$ for ^{232}Th, between 7.4±0.6 and 40.6±1.4 $Bqkg^{-1}$ with a mean of 20.9±1.5 $Bqkg^{-1}$ for ^{226}Ra and between 31.9±1.3 and 114.1±1.4 $Bqkg^{-1}$ with a mean of 69.5±3.2 $Bqkg^{-1}$ for ^{40}K. The values of radioactivity of ^{232}Th and ^{226}Ra are comparable with the global averages of 30 and 35 $Bqkg^{-1}$, respectively, and with those earlier reported for the Kenyan coastline. However, the mean radioactivity concentration of ^{40}K in this investigation was found to be far below the global average of 400 $Bqkg^{-1}$. Therefore, this investigation shows that surface soils in the area around the proposed titanium mines contain low levels of the naturally occurring radionuclides.

The total average effective gamma radiation dose rate from ^{40}K and the progeny of ^{232}Th and ^{226}Ra in the soil has been found to be 62.0±3.5 μSvy^{-1}, which is below the dose limit of 1 $mSvy^{-1}$ for the general public. This dose rate is also below the global normal background level of 460 μSvy^{-1}. The average effective radiation dose rate obtained in this study shows that in the current population of about 3,000 people living in these areas, the number of radiation-induced deaths should be negligible.

6.2 RECOMMENDATIONS

The values of radioactivity of natural radionuclides that have been obtained in this study will be of great use in assessing the future environmental impact of the proposed heavy mineral mining in Msambweni division, Kwale district. However, the study of the radioactivity of soil alone may not result in complete description of the radiological state of an environment. It is, therefore, recommended that the other environmental materials, e.g., air and water in these areas be analyzed for radioactivity and quality parameters prior to the commencement of large-scale mining operations.

A numerical simulation of spatial and vertical distribution of the radionuclides in the soil depth profile up to 40 m, where heavy sands are concentrated, is also recommended.

References

Adams and Dams, 1970. *Applied Gamma-Ray Spectrometry*. Pergamon Press. Pp 217-244.

ARPANSA, 2004. *Ionizing Radiation and Health.* Australian Radiation Protection and Nuclear Safety Agency, Yallambie.

ARPANSA, 2006. *Ionizing Radiation Survey of RMIT Business Building 108.* Australian Radiation Protection and Nuclear Safety Agency, Yallambie.

Austromineral GmbH, 1978. *Geological Survey of Mineral and Base Metal Prospecting in the Coastal Belt, South of Mombasa (Kwale District).* Mines and Geology Department, Ministry of Natural Resources, Kenya. Pp 25-26, 98.

Costal and Environmental Services (CES), 2000. *Environmental Impact assessment, Kwale Titanium Mines Project, Kenya*, **Vol.7**. Summary Report. Pp 14.

Czeizel, A., 1988. *Multiple Congenital Abnormalities.* Akademia Kiado, Budapest. Pp27.

Derbertin, K. and Helmer, R. G., 1988. *Gamma and X-Ray Spectrometry with Semi-conductor Detectors.* North-Holland-Elsevier, Amsterdam. Pp 399.

Emden, B. V., Thornber, M. R., Graham, G., Lincoln, F. J., 1997. *The Incorporation of Actinides in Monazite and Xenotime from Placer Deposits in Western Australia.* The Canadian Mineralogist **35**. Pp 95-104.

Gramaccioli, C. M., Segalstad, T. V., 1978. *A Uranium- and Thorium-Rich Monazite from a South-Alpine Pegmatite at Piona, Italy.* American Mineralogist **63**. Pp 757-761.

Hashim, N. O., Rathore, I. V. S., Kinyua, A.M. and Mustapha, A. O., 2004. *Natural and Artificial Radioactivity Levels in Sediments along the Kenyan Coast.* Radiation Physics and Chemistry, **Vol. 71**. Pp 805-806.

IAEA, 1987. *Preparation and Certification of IAEA Gamma Spectrometry Reference Materials.* International Atomic Energy Agency, **IAEA/RL/148**, Vienna.

IAEA, 1989. *Measurement of Radionuclides in Food and Environment. A Guidebook.* Technical report Series **No. 295**. IAEA, Vienna. Pp 22-66.

IAEA, 1991. *Gamma-Ray Spectra Analysis, Activity Calculations and Neutron Activation Analysis Software (GANAAS).* IAEA, Vienna

ICRP, 1991. *Annual Limits on Intake of Radionuclides by Workers Based on 1990 Recommendations.* International Commission on Radiological Protection. Publication **no. 61**, Annals of the ICRP **21(4).**

Japanese International Cooperation Agency, JICA (1993). *Report on Mineral Exploration in Mombasa Area – Consolidated Report.* Mines and Geology Department, Ministry of Natural Resources, Kenya. **Report Number 30**, pp 102-117, 132-133.

Jelfs, P., 1992. *Cancer in Australia 1983 – 85.* Australian Institute of Health and Welfare. Cancer Series **1**, Pp101. Australian Government Printing Service.

Knoll, G. F., 1989. *Radiation Detection and Measurement.* John Wiley and Sons, New York.

Kohshi, C., Takao, I., Hideo, S., 2001. *Terrestrial Gamma Radiation in Kohshi Prefecture, Japan.* Journal of Health Science **47(4).** Pp 362-372.

Mohanty, A. K., Sengupta, D., Das, S. K., Saha, S. K., and Van, K. V., 2004a. *Natural Radioactivity and Radiation Exposure in the High Background Area at Chhatrapur Beach Placer Deposit of Orissa, India.* Journal of Environmental Radioactivity **Vol. 75.** Pp 15-33.

Mohanty, A. K., Sengupta, D., Das, S. K., Vijayan, V., and Saha, S. K., 2004b. *Natural Radioactivity in the Newly Discovered High Background radiation Area on the Eastern Coast of Orissa, India.* Radiation Measurements vol. **38.** Pp 153-165.

Mustapha A. O., Patel, J. P., and Rathore, I. V. S., 2000. *Assessment of Human Exposure to Natural Sources of Radiation in Kenya.* Radiation Protection Dosimetry, **vol. 82**. Pp 285-292.

Narayana, Y., Somashekarappa, H. M., Karunakara, N., Avadhani, D. N., Mahesh, H. M., Sidappa, K., 2000. *Prominent Artificial Radionuclide Activity in the Environment of Coastal Karnataka on the Southwest Coast of India.* Journal of Radiological Protection, **Vol.20**. Pp 295-300.

Ong'olo, D., 2001. *International Investment and Environmental Issues: The Case of Kenya's Kwale Mineral Sands Project.* Cuts Investment for Development (IFD). Lusaka, Zambia.

Overstreet, W. C., 1967. *The Geological Occurrence of Monazite*. U S Geological Survey Professional Paper, **530**. Pp 327.

Patel, J. P., 1991. *Environmental Radiation Survey of the Area of High Natural Radioactivity of Mrima Hill of Kenya.* Discovery and Innovation, **vol.3, No. 3**. Pp 31-35.

Radiation Information Network, 2004. *Radioactivity*. Idaho State University, USA.

Tzortzis, M. and Tsertos, H., 2004. *Determination of Thorium, Uranium and Potassium Elemental Concentrations in Surface Soils in Cyprus*. Journal of Environmental Radioactivity, **Vol. 77**. Pp 325-338.

Tzortzis, M., Tsertos, H., Christofides, S., Christodoulides, G., 2003. *Gamma-ray Measurements of Naturally Occurring Radioactive Samples from Cyprus Characteristic Geological Rocks*. Radiation Measurements, **vol. 37**. Pp 221 –229.

United Nations Environment Programme, 1985. *Radiation: Doses, Effects, and Risks.* United Nations Environment Programme, Nairobi.

United Nations Environment Programme, 1999. Global Environmental Outlook 2000 – UNEP's Millennium Report on the Environment. Earth Scan Publications Ltd. London, UK. Pp 398.

UNSCEAR, 1988. *Sources of Ionizing Radiation.* United Nations Scientific Committee on Effects of Atomic Radiation, United Nations, New York.

UNSCEAR, 1993. *Sources of Ionizing Radiation.* United Nations Scientific Committee on Effects of Atomic Radiation (UNSCEAR) 1993 report, United Nations, New York.

UNSCEAR, 2000. *Sources and Effects of Ionizing Radiation.* Report to General Assembly, with Scientific Annexes, United Nations, New York.

Zaman M. B., Hayumbu, P., and Munsanje, S. S., 1993. *Gamma Spectroscopic Measurements of Natural radioactivity in Zambian Phosphate Ores and Products.* International Journal of BioChemiPhysics, **vol. 2, Nos. 1 &2.**

Appendices

APPENDIX 1: Gamma-ray spectrum of the calibration standard (SRM-1)

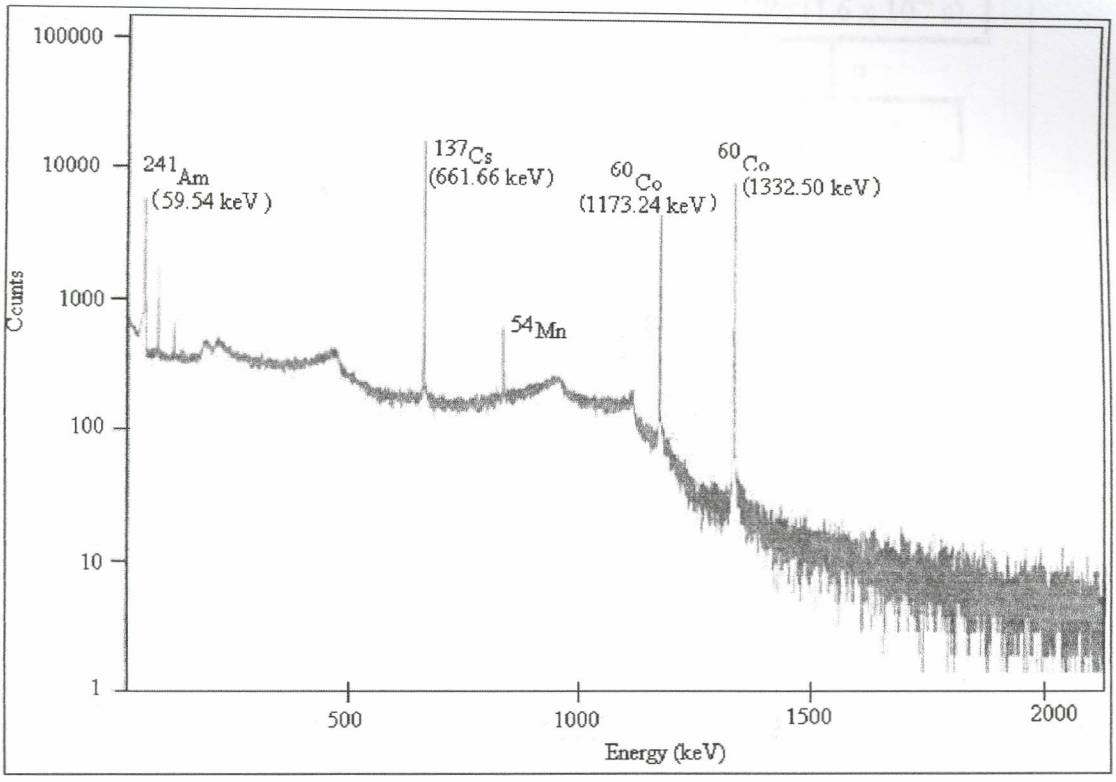

APPENDIX 2: Uranium-238 (^{238}U) decay series

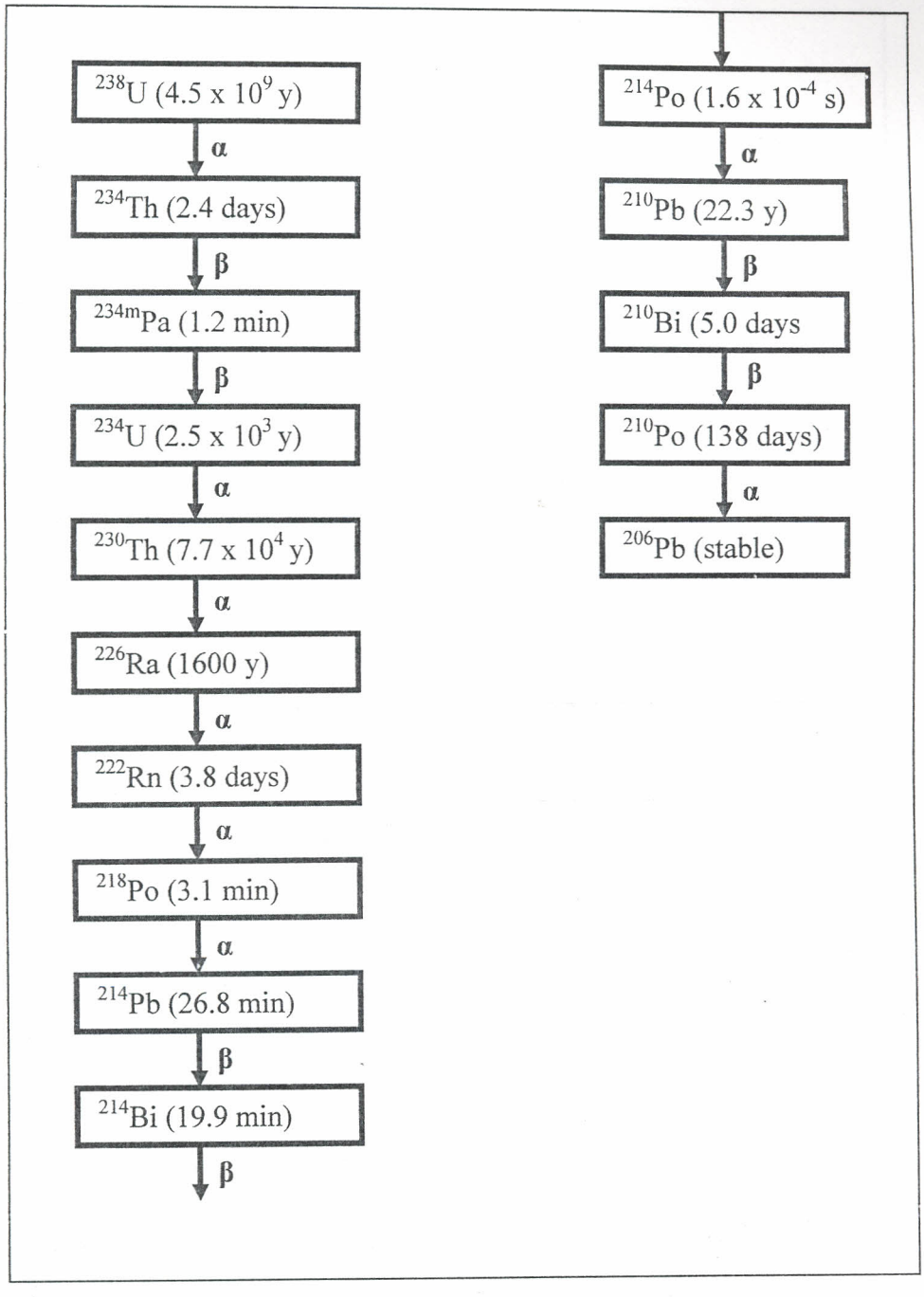

APPENDIX 3: Thorium-232 (^{232}Th) decay series

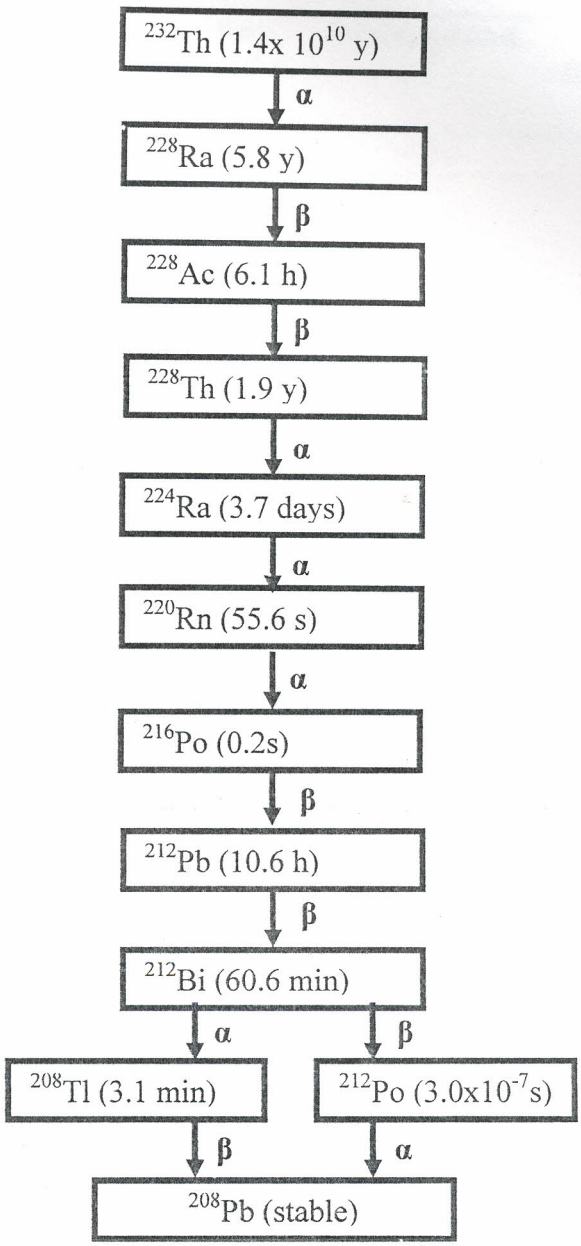

APPENDIX 4: Typical spectrum report of a soil sample analyzed by HpGe detector-based Gamma ray spectrometer

PEAK No.	ENERGY keV	FWHM	Net area	Background	Net Counts/s	%Error
01	27.56	2.19	22190	3456	0.417	1.04
02	77.30	4.13	2096	6092	0.039	13.12
03	93.25	1.42	1087	6120	0.020	23.55
04	106.65	1.68	333	3467	0.006	49.25
05	209.94	0.72	371	2180	0.007	30.73
06	239.11	2.05	4092	2059	0.077	4.10
07	295.85	2.24	923	2987	0.017	19.61
08	338.78	1.85	588	2210	0.011	19.61
09	352.56	2.26	1556	1725	0.029	0.23
10	511.77	3.38	1541	1269	0.029	7.72
11	559.16	2.46	267	799	0.005	20.46
12	583.96	2.08	880	1071	0.017	11.25
13	610.24	2.20	1069	1057	0.020	9.17
14	728.01	1.62	175	687	0.003	42.29
15	912.27	2.36	679	517	0.013	10.60
16	1121.74	2.46	245	367	0.004	30.85
17	1462.07	3.09	545	204	0.010	9.17
18	1765.46	2.53	191	127	0.004	17.80